EFFECT OF MALDISTRIBUTION AND FLOW ROTATION ON THE SHELL SIDE HEAT TRANSFER IN A SHELL AND TUBE HEAT EXCHANGER

A Thesis by

Yaamunan Venkatesan

B. E Mechanical Engineering, Anna University, India 2008

Submitted to the department of Mechanical Engineering
and the faculty of the Graduate school of
Wichita State University
in partial fulfillment of
the requirements for the degree of
Master of Science

May 2011

EFFECT OF MALDISTRIBUTION AND FLOW ROTATION ON THE SHELL SIDE HEAT TRANSFER IN A SHELL AND TUBE HEAT EXCHANGER

The following faculty members have examined the final copy of the Thesis for form and content and recommend that it be accepted in partial fulfillment of the requirement for the degree of Master of Science with a major in Mechanical Engineering.

T.S. Ravigururajan, Committee Chair

Ramazan Asmatulu, Committee Member

Krishna Krishnan, Committee Member

DEDICATION

To my family and friends

ACKNOWLEDGEMENTS

I would like to express my sincere gratitude to Dr. T.S. Ravigururajan, who has guided me towards the successful completion of this research work. I would also like to thank my committee members for taking their time off their busy schedules in reviewing my thesis.

I would also like to acknowledge the support of my friends particularly Rohitha Paruchuri and Aneesha Gogineni in the completion of this thesis. Special thanks to my friend Deepa Jayaraman for being with me throughout the course of my thesis.

ABSTRACT

A numerical analysis of flow maldistribution and shell side flow on heat in a shell and tube heat exchanger is presented. The flow field at the inlet and in the headers was obtained by solving conservation equations of mass and momentum by employing k-ε turbulence model. As the flow maldistribution in the header affects the heat transfer performance of the STHE, pressure drop and velocity distribution of the fluid inside the header were analyzed. Two types of headers were considered with varying header length for a Reynolds number range of 1000 to 3000. As the header length was increased to 1500 mm the flow maldistribution decreased and the static pressure was almost equal for all the tubes in case of a conical header. Also, the numerical simulations show that the conical header with 1500 mm header length has less flow maldistribution when compared to other models. The Shell side flow was modeled as a flow along a twisted tube with a diameter D and a length 30D using Catia V519. Four different models of the twisted tube with pitch varying between 4D and 5.5D were studied for a range of Reynolds number Re = 75-750. The analysis was carried out for three different wall temperatures of the twisted tube such as 343 K, 363 K and 383 K. The pressure drop increased with increase in Reynolds number, while the pressure drop and outlet fluid temperature increased with decrease in the pitch of the tube. But the convective heat transfer decreased with reduction in pitch. With a decrease in pitch, the energy transfer between the fluid and the adjacent tubes increases resulting in increased outlet fluid temperature.

TABLE OF CONTENTS

TABLE OF CONTENTS (cont.)

LIST OF FIGURES

Figure **Page**

LIST OF FIGURES (cont.)

Figure **Page**

LIST OF TABLES

NOMENCLATURE

C_{1E} (constant) = 1.44 (Eq 10)

C_{2E} (constant) = 1.92 (Eq 10)

C_{3E} (constant) = 0.09 (Eq 10)

G_K generation of turbulence kinetic energy due to the mean velocity gradients (Eq 9)

G_b generation of turbulence kinetic energy due to buoyancy Eq (9)

Re Reynolds number

Y_m contribution of the fluctuating dilatation in compressible turbulence to the overall dissipation rate.

σ_K turbulent Prandtl numbers for K = 1.0 (Eq 9)

σ_E turbulent Prandtl numbers for ε = 1.3 (Eq 10)

ε Dissipation rate

K turbulence kinetic energy

ρ density of the fluid. (kg/m^3)

μ kinematic viscosity of the fluid. (m^2/s)

{u,v,w} fluid flow velocity components (m/s)

{r,θ, z} cylindrical coordinates

β thermal volumetric expansion coefficient k^{-1}

t time (s)

r residual, radial coordinate

θ angular coordinate

c_p specific heat kJ/kgK

g gravitational force (N/m^2kg^2)

NOMENCLATURE (cont.)

P	pressure (Pa)
T	temperature (K)

CHAPTER 1

INTRODUCTION

Shell and tube heat exchangers are widely used heat exchangers in process industries, in conventional and nuclear power stations as condensers, steam generators in pressurized water reactor power plants, and feed water heaters. They can also be used for many alternative energy applications including ocean thermal energy and geothermal energy. Tubular heat transfer surfaces are easy to construct in a wide range of sizes and are mechanically rugged enough to withstand the fabrication stresses and high temperatures and pressure operating conditions. They can be easily cleaned and the failure parts like gaskets and tubes can be easily replaced. Figure 1 represents a Shell and tube Heat exchanger [1]. These exchangers are built of round tubes mounted in a cylindrical shell with the tubes parallel to the shell. One fluid flows inside the tubes and the other fluid flows across and along the axis of the exchanger. Shell and tube Heat exchangers can be designed for high pressure relative to the environment and high pressure difference between the fluid streams [2-4]. The basic components of a shell and tube heat exchangers are tubes, tube sheets, shell and shell-side nozzles, tube side channels and nozzles, channel covers, pass divider and baffles. Recently, the tubes are manufactured as twisted tubes instead of conventional tubes. The reason for this is the higher heat transfer characteristics that these twisted tubes can offer and an alternative to baffle based design.

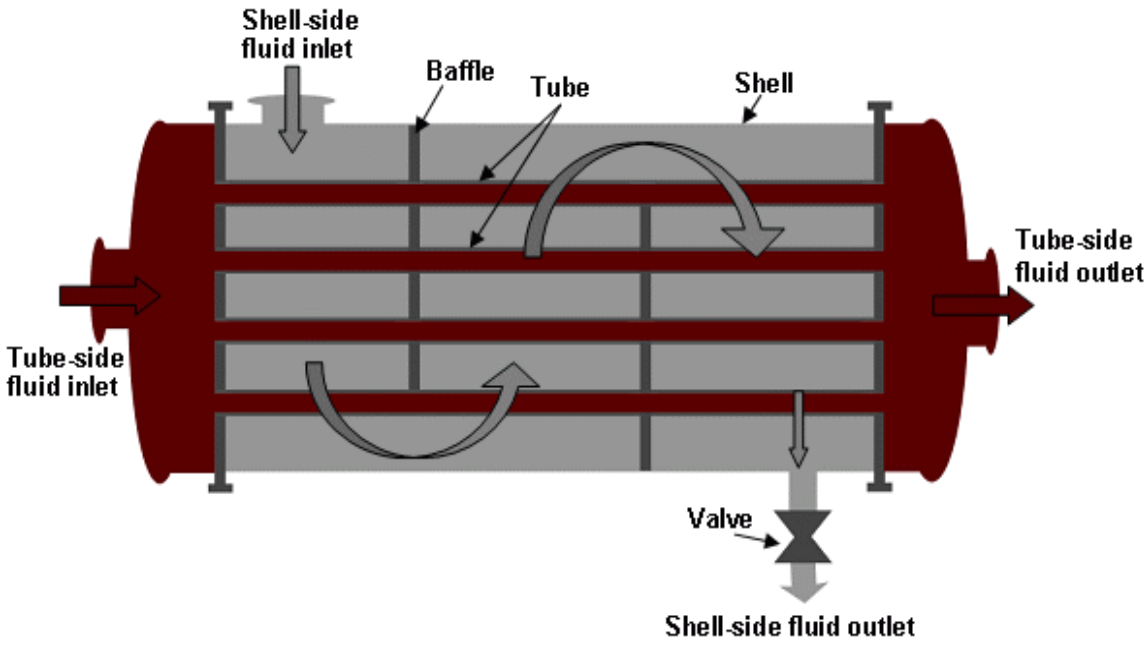

Figure 1. Representation of a shell and tube heat exchanger [1].

CHAPTER 2

BACKGROUND AND LITERATURE REVIEW

2.1 Flow Maldistribution in Header

The important assumption in basic heat exchanger design is based on the uniform distribution of flow at the inlet of the heat exchanger on each fluid side and throughout the core. But in general it is not uniform and maldistribution of flow leads to lower heat transfer performance [5, 6]. For a tube side flow through a bundle of tubes, uniform distribution means equal amount of fluid in each tube or that each particle of fluid has an equal residence time in each tube. However, this fluid flow can be at different rates [7] mainly due to two phase flow distribution, fouling/corrosion effects, heat transfer process itself like viscous flow coolers or thermo acoustic oscillations maldistribution can also be caused by mechanical issues due to the design of headers and inlet ducts acting upon the flow distribution or manufacturing tolerance effects in compact type exchangers. Patankar and Spalding [8] simplified a three dimensional STHX to a porous media model and they introduced the concept of distribution resistance to simulate STHX.

A 3D model for heat transfer in tube bundles in shell and tube heat exchangers was developed by Butterworth [9]. Mueller and Chiou [10] explained in detail the various types of flow maldistributions in heat exchangers and how it affects the performance as well as the causes of these maldistributions of the heat exchanger. They concluded that the flow maldistribution is the major factor affecting heat-transfer performance on the average effective temperature difference and that variation of coefficient is a minor factor. They have also concluded that thermal performance of the exchanger was found to depend on the degree of maldistribution and its cause. Fraas et al [11] described the

extent of maldistribution using the velocity ratio between maximum and minimum values in tube. The effects of inlet fluid flow non-uniformity on thermal performance and pressure drops were investigated by Ranganayakulu et al. [12] in cross flow plate-fin heat exchangers. The analysis was carried out using a finite element model.

Zhang et al. [13-14] did experimental study on heat transfer enhancement of a helically baffled heat exchanger. Zhang investigated the flow maldistribution in plate fin heat exchangers [15]. Experimental studies of shell-and-tube heat exchangers with the same shell-side pressure drop with continuous helical baffles and conventional segmental baffles was carried out by Peng et al. [16] .They concluded that the use of helical baffles results in nearly 10% increase in heat transfer coefficient when compared to that of conventional segmental baffles. Experimental results of pressure drop and heat transfer of a heat exchanger with helical baffles was presented by Lei et al. [17]. Even though experiment research can provide reliable test data for designers and researchers, it is very expensive and time consuming. So, compared to experiment, a validated CFD method can provide more information in heat exchangers at much lower cost and time. Prithiviraj and Andrews [18–20] developed a three-dimensional CFD method to simulate flow and heat transfer in shell and tube heat exchangers with volumetric porosities and surface permeabilities. The flow and heat transfer in shell side of Shell and tube heat exchanger based on the method proposed by Prithiviraj and Andrews [18-20], and the accuracy of numerical model results was validated by experimental data was investigated by Deng [21]. Andrews and Master [22,23] in 2005 used HEATX method to investigate the performance of a Shell and tube heat exchanger. Their computed pressure drops results compared reasonably well with Lummus Heat Transfer Co. pressure drop correlation

results. Two- and three-dimensional simulation models for the computation of flow-induced vibration of tube bundles were applied by Schroder and Gelbe [24]. 2D CFD calculations for condensation rate of a pure refrigerant in vapor flow field and a binary mixture in a shell-and-tube condenser was calculated by Karlsson and Vamling [25]. Lee and Hur [26] investigated the flow and heat transfer effects in the shell side of a Shell and tube heat exchanger, the effects of sizes and locations of the sealing strips were also investigated in their study. Shen et al. [27] established a mathematical model to simulate the influence of helical baffles on heat transfer and flow characteristics in a shell and tube heat exchanger. At the 35^0 helix inclination angle the numerical simulation results were compared with experimental data. Lei et al. [28] investigated the effects of helix angles on flow and heat transfer characteristics of Shell and tube heat exchangers with continuous baffles. Jafari Nasr and Shafeghat [29] studied the velocity distribution in Shell and tube heat exchangers at different helix angles and developed a rapid algorithm for design.

Several studies [30-32] investigated the flow maldistribution effects in plate and cross flow heat exchangers. Ratts [33] investigated the effect of flow maldistribution on the performance of a laminar, counter flow, high-effectiveness heat exchanger. The parameters of fluidization distribution into operating parameters, such as heat quantity in each pipe, mass flux, geometric parameters etc was classified by Vist et.al [34]. Lalot et al [35] did experimental and computational works for velocity distribution in an electric heater. They came to a conclusion that the computed velocity ratio (maximum velocity/minimum velocity) deviated from the experimental results.

2.2 Twisted tube – Shell side flow

Heat transfer in mini and microchannel has important applications in electric energy and automotive mini/micro heat exchangers. One of the main reasons for this is the high heat transfer coefficients that these geometries offer. Numerical study of fluid flow and heat transfer in microchannel cooling passages was studied by Jiang-Tao and Xiao-Feng [36]. The variation of heat transfer coefficient with respect to velocity is shown. Jung-Yeul Jung and Ho-Young Kwak [37] studied the fluid flow and heat transfer in microchannels with rectangular cross section. Pressure drop and temperature variation along the length of the channel was studied. For this study microchannel with different widths from 100, 150 and 200 μm with same height was considered. Garimella et al [38] investigated the heat transfer through rectangular microchannel.

They analyzed a 3d model of the microchannel for this reason and the experimental results were compared against conventional correlations to evaluate their applicability in predicting microchannel heat transfer. Single-phase convective heat transfer in microchannels was reviewed by Luca Morini et al [39]. The analysis conducted in this review was to understand the fluid flow and the heat transfer mechanisms in microchannels. An experiment to determine the heat transfer and pressure drop in narrow rectangular channels was conducted by Momoda et al [40]. The data for heat transfer and pressure drop were obtained and the correlation for the two phase pressure drop was obtained. Beaupre et al [41] gave a paper on Microchannel takes heat sink to next level. Heat transfer in microchannel heat sink was studied through CFD software. Zummo et al [42] studied the Microtube liquid single-phase heat transfer in laminar flow. Here the single phase heat transfer of micro tubes was studied for laminar

flow. The size effect on single phase channel flow and heat transfer at micro scale was studied by Zhi-Xin Li et al [43]. The effect of axial conduction on the heat transfer of a triangular microchannel was analyzed by Tiselj et al [44]. For this reason the channel was heated from three faces. It was shown that as the bulk water temperature as well as the temperature of the heated wall, do not change linearly along the channel. Mudawar et al [45] analyzed three dimensional heat transfers in microchannel heat sinks.

The use of flow visualization in micro and minichannel geometries for the development of pressure drop and heat transfer models during condensation in refrigerants (R134 a) was investigated by Garimella [46]. Coleman and Garimella [47] investigated the effect of tube diameters on flow patterns for air-water mixture flow in round and rectangular shaped microchannel of hydraulic diameter 1.3-5.5mm. The film condensation heat transfer inside vertical mini triangular channels was analyzed by Zhao and Liao [48]. They found that the condensation heat transfer coefficient in a triangular tube is higher than that of a round tube. Other experimental data [49, 50] also showed that the condensation heat transfer in mini/microchannels is different from those in macrochannels. Wang et al [49] found that, existing correlations over predicted the heat transfer in a horizontal rectangular multi-port aluminum condenser tube of 1.46 mm hydraulic diameter. An experimental investigation of R134a condensing inside a single round tube with an inner diameter of 0.691 mm was done by Kim et al [50]. They found that the existing heat transfer correlations failed to predict their data, and discrepancies become more obvious especially at low mass fluxes. Yang and Webb [51] obtained heat transfer coefficients for condensation of R12 and subcooled liquid in small tubes of hydraulic diameter of 16mm. A technique for the measurement of condensation heat

transfer coefficients in microchannel with hydraulic diameter of 0.76mm was reported by Garimella and Bandhauer [52]. The heat transfer coefficients for condensation of R143a in the tube were in the range of 0.211-1.064 W/cm^2.

K. Fiedler and Auracher [53] conducted experiments to measure the heat transfer coefficient in a tube inclined at an angle of 45^o. The condensation heat transfer coefficient of R134a in minichannels was measured in [54]. During this measurement, Shin and Kim measured the pressure drop and heat transfer coefficient was investigated. Wang et al. [55] proposed a model to compute the film condensation heat transfer coefficient in square minichannel. R134a was the working fluid and the tube diameter was 1mm. Mederic et al. [56] visualized the condensation pattern in a capillary tube with inner diameter and length as 0.56mm and 100mm respectively. An investigation on the local heat transfer coefficient for condensation flow of HCFC-123 and R11 in tubes with inner diameter of 0.92mm and 1.95mm was conducted by Baird et al. [57]. Garimella et al [58] validated a two phase pressure drop model for circular microchannels with hydraulic diameter between 0.5-4.91mm. Louahlia-Gualous and Mecheri [59] studied the unsteady steam condensation in miniature tube. Different patterns of flow were visualized by varying the inlet pressure and cooling rates. The visualization of multi-channel effect in a silicon triple-channel condenser with an aspect ratio of 0.04 was studied by Zhang et al. [60].

An investigation on the heat transfer and flow friction characteristic of steam condensation in silicon microchannels was conducted by Wu et al. [61]. Trapezoidal microchannel with hydraulic diameters of 0.0775mm, 0.093mm and 0.128mm were tested under different flow and cooling conditions. An experimental investigation for

enhancement of heat transfer in a shell and tube heat exchanger was performed by Wang et al. [62]. The gaps between the baffles and shells were blocked using sealers in order to increase the heat transfer on the shell side of the shell and tube heat exchanger. Chen et al. [63] studied the flow and heat transfer characteristics of a combined multiple shell-pass shell- and-tube heat exchangers with continuous helical baffles using CFD. It was studied that under same conditions of mass flow rate and heat transfer rate, the pressure drop was lower for a novel heat exchanger than a conventional segmental baffled heat exchanger. A computer modeling for a shell and tube heat exchanger was simulated by Keene et al. [64] for analyzing the flow distribution on the shell side of a shell and tube heat exchanger. This was done in order to understand the complexities involved in the flow patterns when fluid passes over the tubes in the baffle compartments. Ozden et al. [65] conducted a CFD modeling for a shell and tube heat exchanger. During this study, they analyzed the overall heat transfer coefficient and pressure drop of a single shell and a single tube pass heat exchanger with baffles on the shell side.

The work described in chapter 2.1 is mainly related to the influence of flow maldistribution on the performance of heat exchangers. While the above studies are restricted to elliptical and cylindrical headers, conical headers have not been studied in detail. So, in the present work a 3-D simulation model on flow distribution in a shell and tube heat exchanger header part is presented. Two different header types were considered. One is a circular header and the other one is conical header. The numerical results of the shell and tube heat exchanger simulation will be presented in detail. Specifically more work is focused on pressure distribution and velocity distribution in a

conical and circular header part of shell and tube heat exchanger to see the maldistribution inside the header.

In all the cases explained in chapter 2.2 heat transfer through various geometries at mini/micro level was considered. All of the above cases included baffles on the shell side of a shell and tube heat exchanger. But none of the papers dealt with heat transfer through twisted tubes. The conventional shell and tube heat exchangers use cylindrical tubes with baffles on the shell side. Since there is a growing demand for STHE, it is necessary to reduce the cost incurred on them. One way of doing that is by eliminating the use of baffles. This can be successfully achieved with the use of twisted tubes rather than conventional cylindrical tubes. When twisted tubes are used for STHE, the tubes are held together by the twist formed, thus allowing the shell side coolant to flow through the twists. Since the channel space between these twists tubes are considered to be at the micro level, the author has done a considerable review on flow through mini/micro channels. This paper deals with use of twisted tubes in a STHE and the shell side flow is analyzed using CFD.

2.3 Objectives

- Determine suitable header geometry for minimum flow maldistribution.
- Determine a suitable twisted tube for improved heat transfer characteristics on the shell side.

CHAPTER 3

NUMERICAL THEORY AND PROCEDURE

3.1 Introduction

Steady state flow modeling was performed. For the flow analysis, laminar model and standard k-epsilon turbulence model were approached. The conservation equations of mass and momentum are solved using the finite volume method. The complete models of turbulence are two-equation models in which solution of two separate transport equations allows the turbulent velocity and length scales to be independently determined. The standard k-epsilon turbulence model falls under this category and it is widely used for practical flow modeling calculations.

3.2 Finite Volume Method

Finite volume method was introduced by McDonald (1971) and MacCormack and Paullay (1972) for two-dimensional time-dependent Euler equations and later it was extended to three-dimensional modeling by Rizzi and Inouye (1973). In this method the computational domain was divided into finite number of contiguous control volumes. At each control volume center the variable values were calculated. Interpolation technique was used to show variable values at control volume surface in terms of center values and quadrature formulae are applied to approximate the surface and volume integrals. For each control volume an algebraic equation can be obtained which denotes the number of neighboring nodal values [66].

3.3 Conservation Laws

The flow maldistribution and heat transfer characteristics are both done with 3D cylindrical models, so the generalized mass, momentum equations are given in cylindrical coordinates in the equations mentioned below [67].

Conservation of Mass or continuity equation

$$\frac{\mathbf{1}}{r}\frac{\partial ru}{\partial r}+\frac{\mathbf{1}}{r}\frac{\partial v}{\partial \theta}+\frac{\partial w}{\partial z}=\mathbf{0} \tag{1}$$

Conservation of Momentum in r direction

$$\frac{\partial u}{\partial r}+u\frac{\partial u}{\partial r}+\frac{v}{r}\frac{\partial u}{\partial \theta}-\frac{v^2}{r}+w\frac{\partial u}{\partial z}=-\frac{\mathbf{1}}{\rho}\frac{\partial p}{\partial r}+\nu[\frac{\partial}{\partial r}(\frac{\mathbf{1}}{r}\frac{\partial ru}{\partial r})+\frac{\mathbf{1}}{r^2}\frac{\partial^2 v}{\partial \theta^2}-\frac{\mathbf{2}}{r^2}\frac{\partial v}{\partial \theta}+\frac{\partial^2 u}{\partial z^2}]+g_r\beta(T-To) \tag{2}$$

Conservation of Momentum in θ direction

$$\frac{\partial v}{\partial r}+u\frac{\partial v}{\partial r}+\frac{v}{r}\frac{\partial v}{\partial \theta}+\frac{uv}{r}+w\frac{\partial u}{\partial z}=-\frac{\mathbf{1}}{\rho r}\frac{\partial p}{\partial \theta}+\nu[\frac{\partial}{\partial r}(\frac{\mathbf{1}}{r}\frac{\partial rv}{\partial r})+\frac{\mathbf{1}}{r^2}\frac{\partial^2 v}{\partial \theta^2}+\frac{\mathbf{2}}{r^2}\frac{\partial u}{\partial \theta}+\frac{\partial^2 v}{\partial z^2}]+g_\theta\beta(T-To) \tag{3}$$

Conservation of Momentum in z direction

$$\frac{\partial v}{\partial r}+u\frac{\partial v}{\partial r}+\frac{v}{r}\frac{\partial v}{\partial \theta}+\frac{uv}{r}+w\frac{\partial u}{\partial z}=-\frac{\mathbf{1}}{\rho r}\frac{\partial p}{\partial \theta}+\nu[\frac{\partial}{\partial r}(\frac{\mathbf{1}}{r}\frac{\partial rv}{\partial r})+\frac{\mathbf{1}}{r^2}\frac{\partial^2 v}{\partial \theta^2}+\frac{\mathbf{2}}{r^2}\frac{\partial u}{\partial \theta}+\frac{\partial^2 v}{\partial z^2}]+g_z\beta(T-To) \tag{4}$$

Conservation of Energy

$$\frac{\partial T}{\partial t}+u\frac{\partial T}{\partial r}+\frac{v}{r}\frac{\partial T}{\partial \theta}+w\frac{\partial T}{\partial z}=\frac{k}{\rho c_0}+[\frac{\mathbf{1}}{r}\frac{\partial}{\partial r}(r\frac{\partial T}{\partial r})+\frac{\mathbf{1}}{r^2}\frac{\partial^2 T}{\partial \theta^2}+\frac{\partial^2 T}{\partial z^2}]+S_T \tag{5}$$

The effects of gravity and external forces are neglected in this study, hence the conservation equations are reduced as follows.

Conservation of momentum in r direction

$$\frac{\partial u}{\partial r}+u\frac{\partial u}{\partial r}+\frac{v}{r}\frac{\partial u}{\partial \theta}-\frac{v^2}{r}+w\frac{\partial u}{\partial z}=-\frac{1}{\rho}\frac{\partial p}{\partial r}+\nu[\frac{\partial}{\partial r}(\frac{1}{r}\frac{\partial ru}{\partial r})+\frac{1}{r^2}\frac{\partial^2 v}{\partial \theta^2}-\frac{2}{r^2}\frac{\partial v}{\partial \theta}+\frac{\partial^2 u}{\partial z^2}] \quad (6)$$

Conservation of Momentum in Θ direction

$$\frac{\partial v}{\partial r}+u\frac{\partial v}{\partial r}+\frac{v}{r}\frac{\partial v}{\partial \theta}+\frac{uv}{r}+w\frac{\partial u}{\partial z}=-\frac{1}{\rho r}\frac{\partial p}{\partial \theta}+\nu[\frac{\partial}{\partial r}(\frac{1}{r}\frac{\partial rv}{\partial r})+\frac{1}{r^2}\frac{\partial^2 v}{\partial \theta^2}+\frac{2}{r^2}\frac{\partial u}{\partial \theta}+\frac{\partial^2 v}{\partial z^2}] \quad (7)$$

Conservation of Momentum in z direction

$$\frac{\partial v}{\partial r}+u\frac{\partial v}{\partial r}+\frac{v}{r}\frac{\partial v}{\partial \theta}+\frac{uv}{r}+w\frac{\partial u}{\partial z}=-\frac{1}{\rho r}\frac{\partial p}{\partial \theta}+\nu[\frac{\partial}{\partial r}(\frac{1}{r}\frac{\partial rv}{\partial r})+\frac{1}{r^2}\frac{\partial^2 v}{\partial \theta^2}+\frac{2}{r^2}\frac{\partial u}{\partial \theta}+\frac{\partial^2 v}{\partial z^2}] \quad (8)$$

The Continuity of mass and momentum equations with equations of turbulence model are used for higher flow rate values. The following equation represents the turbulence model equations [68].

$$\frac{\partial}{\partial t}(\rho k)+\frac{\partial}{\partial x_i}(\rho k u_i)=\frac{\partial}{\partial x_j}\left[(\mu+\frac{\mu_t}{\sigma_k})\frac{\partial k}{\partial x_j}\right]+G_k+G_b-\rho\varepsilon-Y_M \quad (9)$$

$$\frac{\partial}{\partial t}(\rho\varepsilon)+\frac{\partial}{\partial x_i}(\rho\varepsilon u_i)=\frac{\partial}{\partial x_j}\left[(\mu+\frac{\mu_t}{\sigma_\varepsilon})\frac{\partial \varepsilon}{\partial x_j}\right]+C_{1\varepsilon}\frac{\varepsilon}{k}(G_k+C_{3\varepsilon}G_b)-C_{2\varepsilon} \quad (10)$$

3.4 Algorithm

The SIMPLE algorithm is used for pressure-velocity coupling and the solution is iterated until convergence was achieved so that the residual for each equation will fall below the value 10^{-3}. In the present study, CFD was used to show the distribution of velocity and pressure inside the header and heat transfer characteristics on the shell side of a STHE. The main objective of this project is to analyze the flow phenomena in the header part of the heat exchanger and to check for maldistribution. With the change in header length how the maldistribution effects was analyzed. Also, the heat transfer characteristics at different pitch levels on the shell side are analyzed.

CHAPTER 4

MODELING & BOUNDARY CONDITIONS

4.1 Flow Maldistribution in Header

Fig 2 shows a schematic representation of conical header part of a shell and tube heat exchanger and Fig 3 represents a circular header part with the main geometrical characteristics listed. The dimensions for both the headers are considered as same. Three dimensional model was generated. The header is of 1.2 m-ID .It has one inlet nozzle with (0.25m-ID).Three header lengths have been considered with L/D as 0.58, 0.75 and 1.25; header consists of 80 tube side outlets with pitch of 109.09mm.

Applying the No slip condition at the walls

$$u = v = w = 0$$

Adiabatic condition

$$\frac{\partial T}{\partial r} = 0 \text{ at } (r = R)$$

At inlet

$$V = \text{constant}$$

The inlet and outlet conditions are corresponding to the average velocity distribution at the inlet and fully developed flow at the outlet [69, 70]. The value of velocity at the inlet is obtained from Reynolds number. Four different values were considered (1000, 1500, 2300 and 2800). The fluid properties are given in table 1.

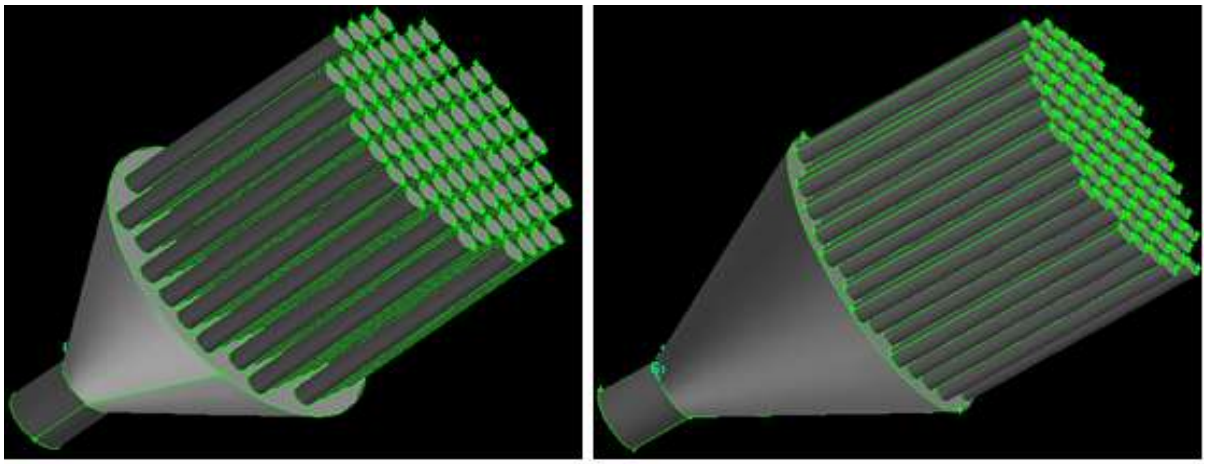

(a) 700mm header length , (b) 900 mm header length

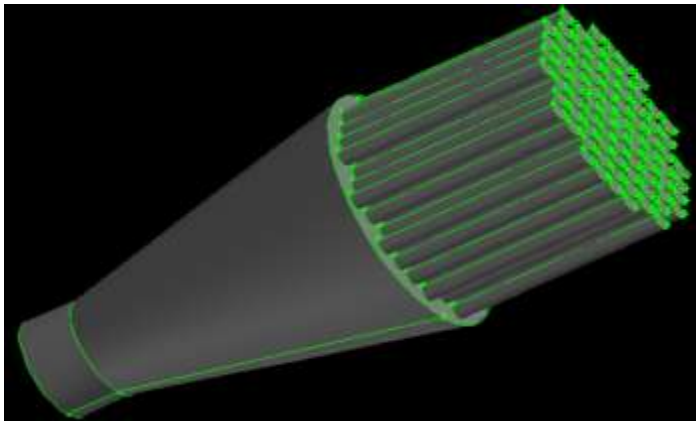

(c) 1500 mm header length

Figure 2. Model of Shell and tube Heat exchanger conical header part.

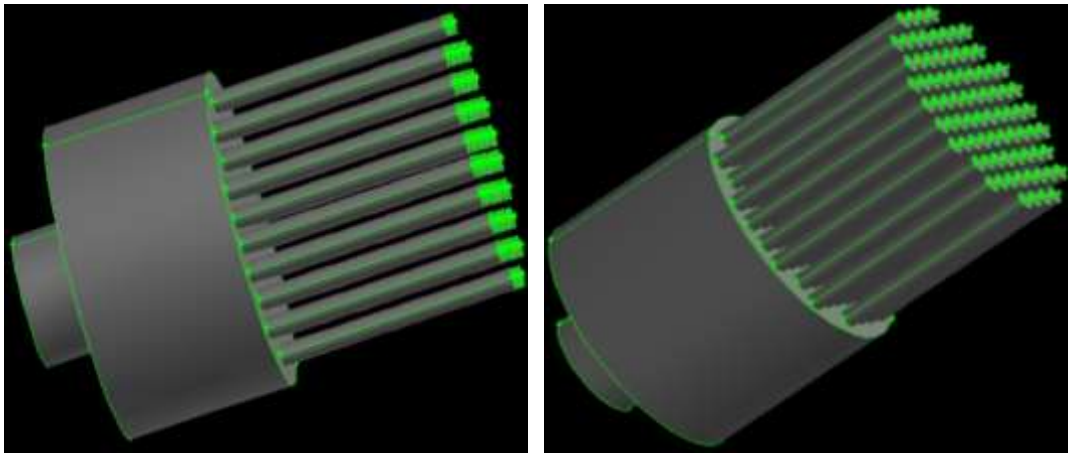

(a) 700 mm header length (b) 900 mm header length

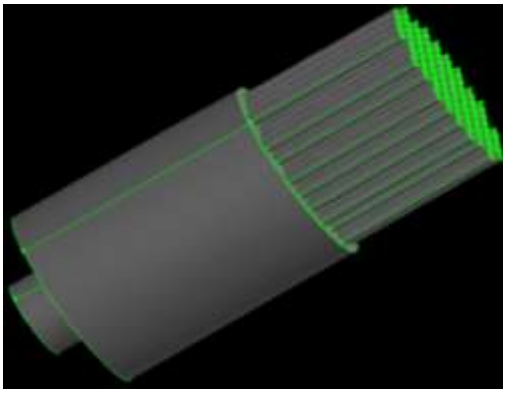

(c) 1500 mm header length

Figure 3. Model of Shell and tube Heat exchanger circular header part.

PROPERTIES	VALUES
Density (Kg/m3)	998.2
Specific heat capacity (J/Kg K)	4182
Thermal Conductivity	0.6
Viscosity (Kg/m s)	0.001003

Table 1: Properties of Water

4.2 Twisted Tube – Shell side flow

The twisted tube model was generated using CATIA V519. The model was generated with a diameter D and length 30D using the helix option. The pitch of the twisted tube was varied as 4D, 4.5D, 5D and 5.5D. The helix angle varied between $50^0$and 65^0 respectively. The model was then imported to GAMBIT, where grids were generated. The model was then exported to FLUENT for the analysis. The model of the twisted tube can be seen in Figure 4 & 5.

The boundary conditions were specified to the twisted tube in order to show the initial state of flow and heat transfer process. The boundary conditions for the microchannel are as follows.

Applying the No slip condition at the walls

$$u = v = w = 0$$

Non-Adiabatic condition

$$\frac{\partial T}{\partial \theta} = \text{Constant}$$

At inlet

$$V = \text{constant}$$

The inlet temperature of the cold fluid on the shell side was constant at 300 K. Temperature of the hot fluid was varied between 343 K and 383 K. In order to obtain the most accurate results the grid was made denser every time until grid independence was achieved.

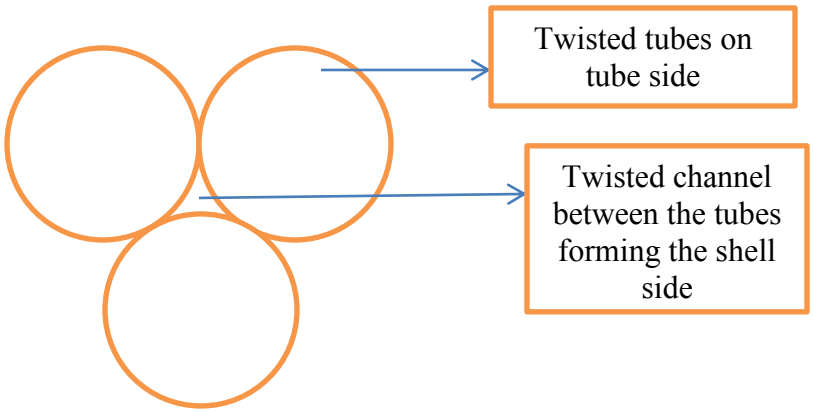

Figure 4. Schematic representation of arrangement of tubes in STHE.

The twisted channel between the tubes is modeled in Catia and is shown in Figure 5.

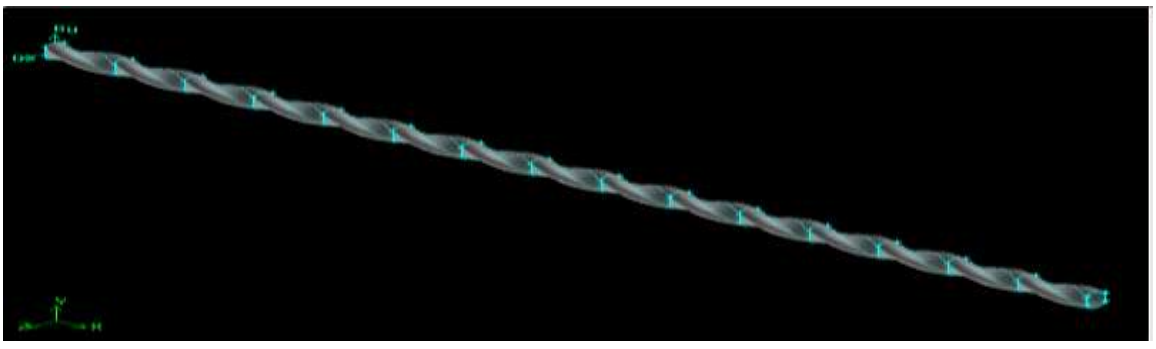

Figure 5. Model of the twisted tube in Catia with pitch of 4D.

CHAPTER 5

RESULTS AND DISCUSSION

5.1 Flow Maldistribution in Header

The results of the velocity contours and vectors of static pressure inside the circular and conical header types are presented. For two different types of headers the header length and flow rate is varied. And the results are compared for both the cases. Analysis is carried out to find out the maldistribution inside the header part of heat exchanger. Water was used as the working fluid with flow Reynolds number ranging from 1000 to 3000. Three different header lengths of 700 mm, 900 mm and 1500 mm were considered for analysis.

5.1.1 Velocity distribution in the header

Fig 6 represents the velocity vectors inside the conical header part and Fig 7 represents the velocity vectors inside a circular header part. It is clearly shown in Figure 6 (a) and Figure 6 (b) that velocity distribution in the header is not uniform. The velocity of fluid at the entrance to the tubes does not seem to be uniform and there is a lot of variation in the values. In Figure 6 (a) the velocity of the fluid is high at the center of the header near the entrance to the tubes and very less towards the corner. Similar reults were obtained in Figure 6 (b) though the distribution of velocity was slightly better. The velocity is very high at some tubes than in other tubes; this is because of the flow maldistribution. Flow maldistribution was greatly reduced for conical headers with L/D = 1.25. The velocity of the fluid was more or less similar at the entrance to all the tubes. It was quite evident from this that increase in header length yielded better flow distribution among the tubes. Figure 7 (a), (b) & (c) represents the velocity distribution of fluid in

circular headers. Similar results were obtained for circular headers as well. Interestingly, the maldistribution was higher in circular headers when compared with conical headers for a specific L/D ratio. In order to obtain the effect of inlet velocity of fluid on mal distribution, a ratio of inlet velocity to the velocity at the tube entrance was calculated and a graph was plotted between that and Flow rate. Figure 8 is a graph that depicts the variation of velocity ratio with respect to flow rate for conical and cylindrical headers. Figure 8 (a) shows the variation for a conical header and it is clear that with increase in the inlet velocity the average velocity at the tube entrance increases. The velocity ratio was maximum at 0.6 for a conical header at a high Reynolds number of 3000. It was also clear that at high Reynolds number (flow rate) the velocity of fluid at each tube entrance was approximately equal. Figure 8 (b) shows the same variation for a circular header and the maximum value of velocity ratio was obtained as 0.45. From this we can clearly see that the flow is not uniform and maldistribution of flow takes place leading to low heat transfer performance. For a circular header the velocity distribution is not uniform and for all the header models the ratio of velocity at the inlet to the velocity of fluid entering the tubes is in the range of 0 to 0.45. From Fig 8 we can conclude that conical header with header length of 1500mm has uniform flow distribution when compared to the other cases. As the header length is increased to 1500mm in conical header model the flow maldistribution was reduced by about 83.3%.

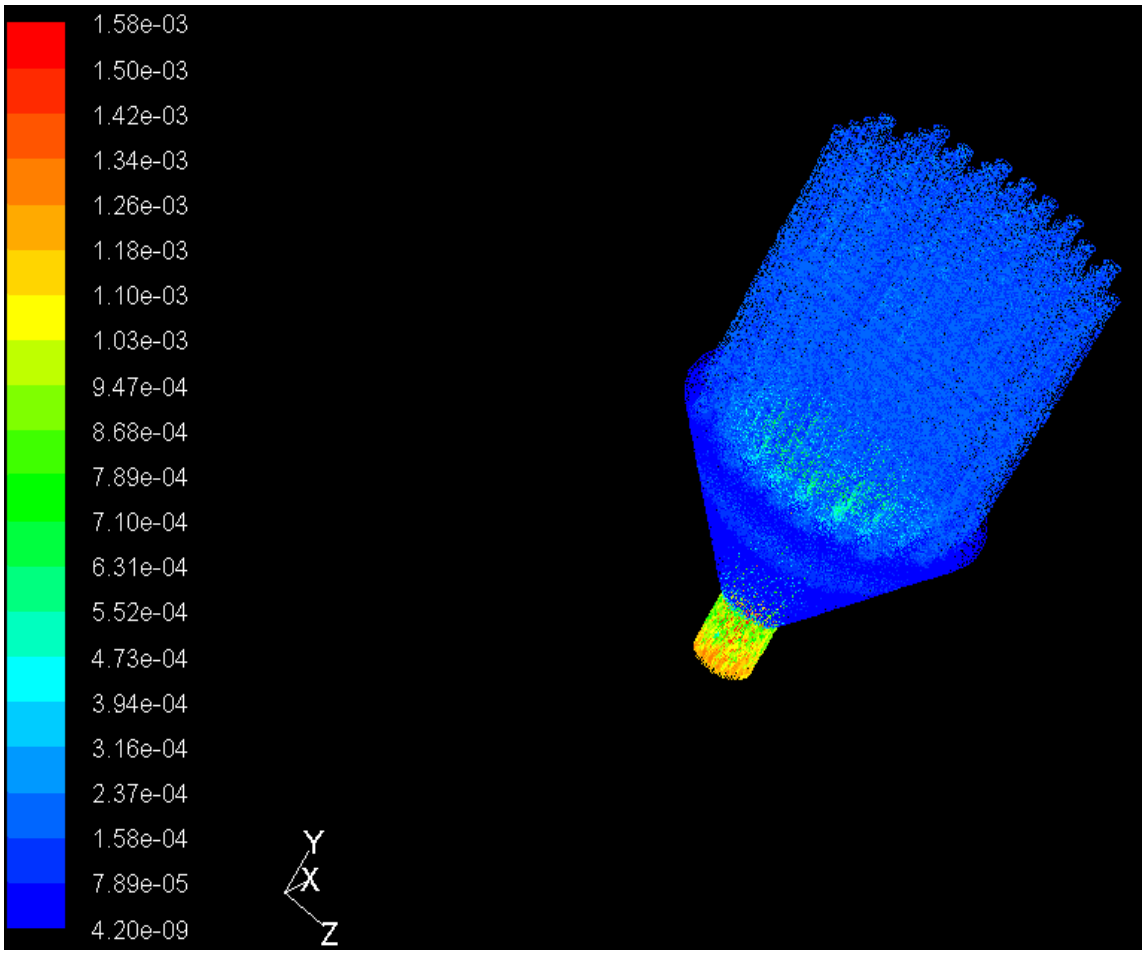

Figure 6 (a). Velocity distribution inside the conical header of L/D = 0.58 with flow rate of Re=1500.

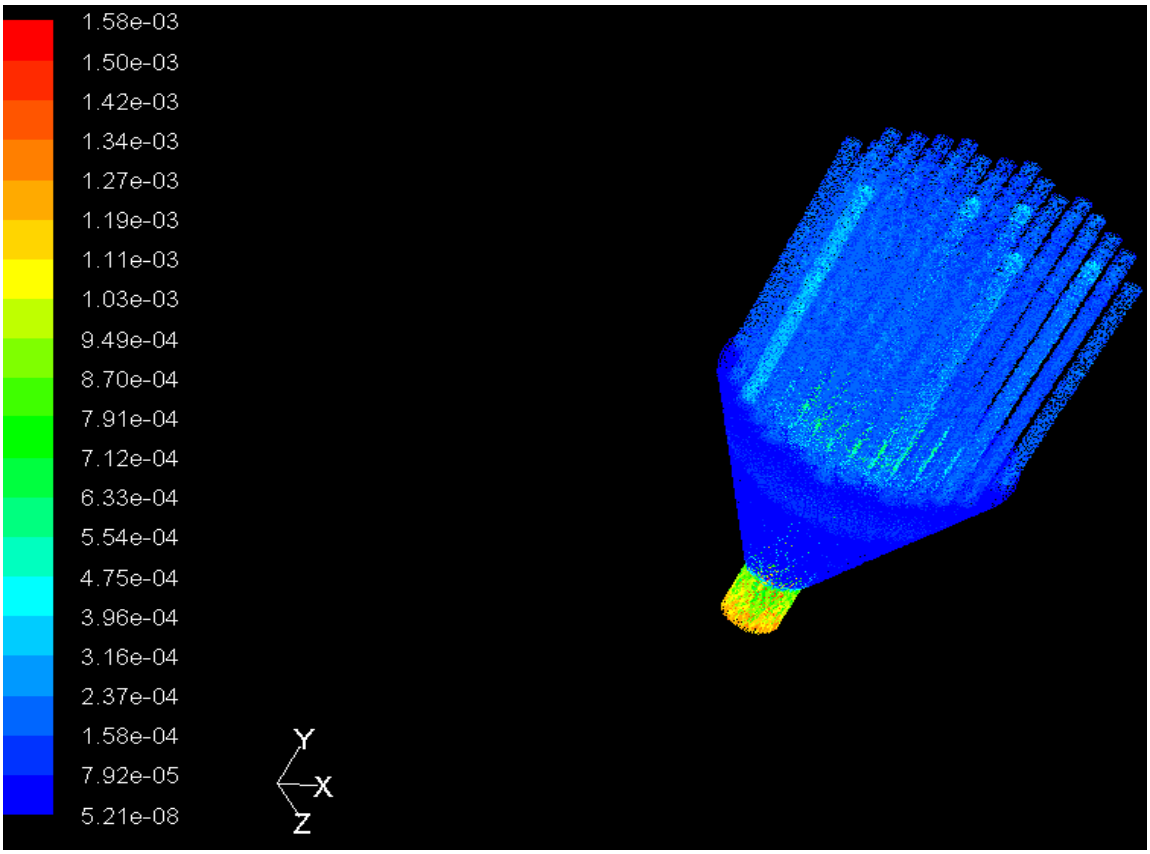

Figure 6 (b). Velocity distribution inside the conical header of L/D = 0.75 with flow rate of Re=1500.

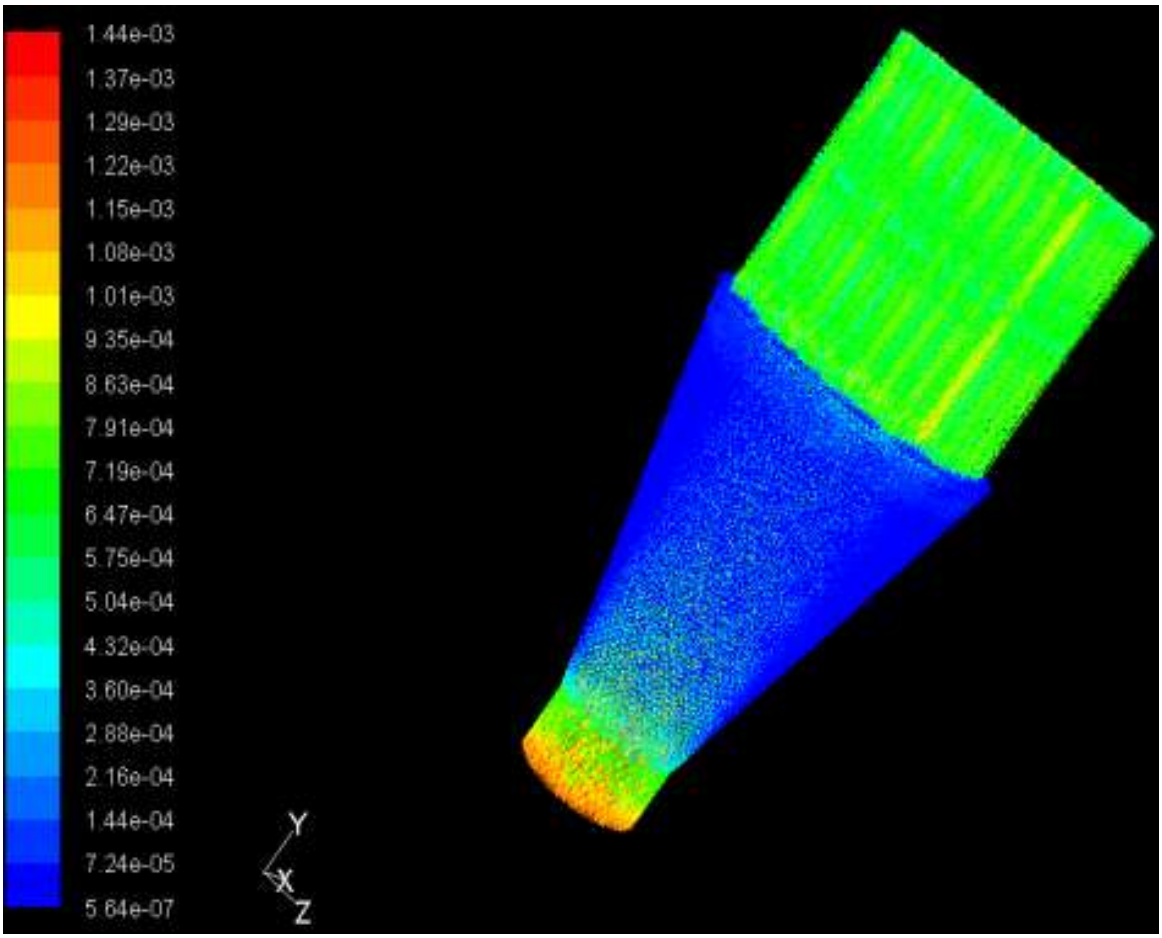

Figure 6 (c). Velocity distribution inside the conical header of L/D = 1.25 with flow rate of Re=1500.

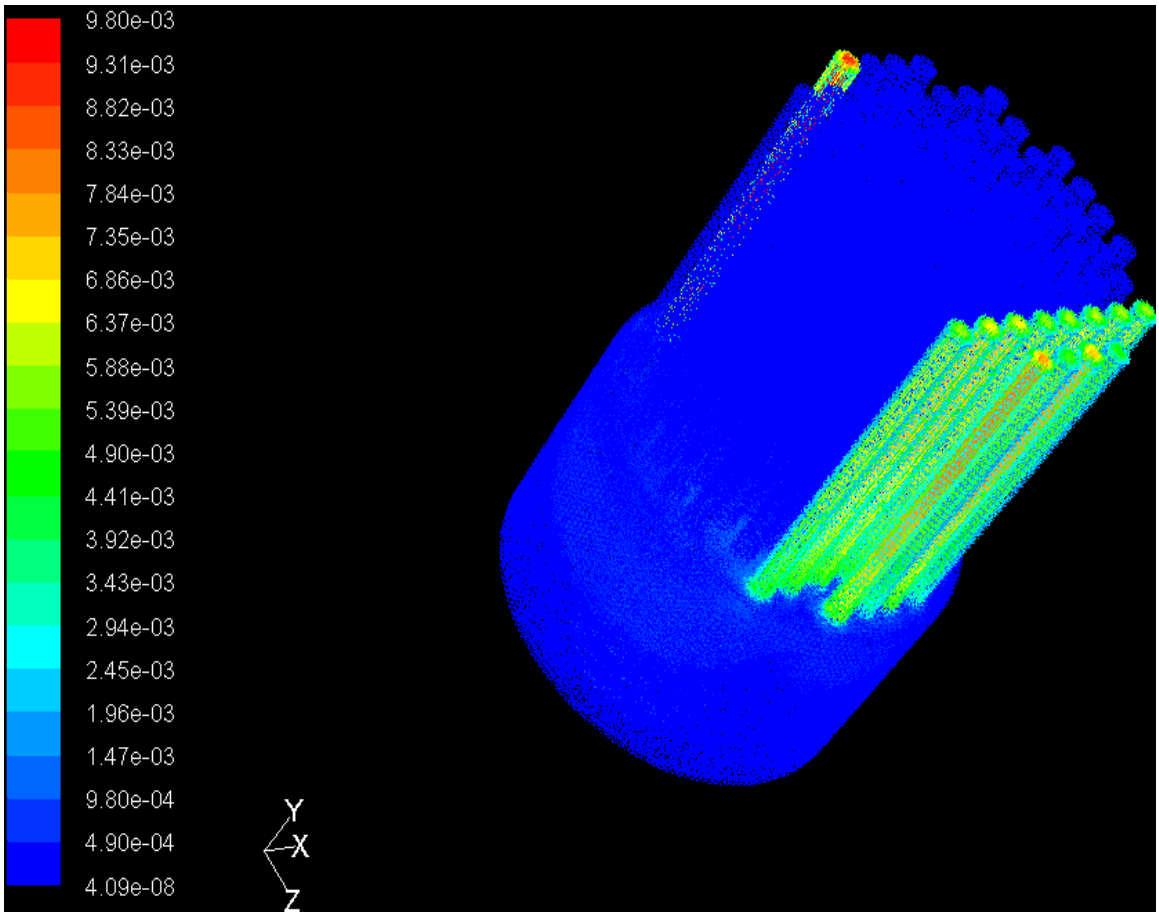

Figure 7 (a). Velocity distribution inside the cylindrical header of L/D = 0.58 with flow rate of Re=1500.

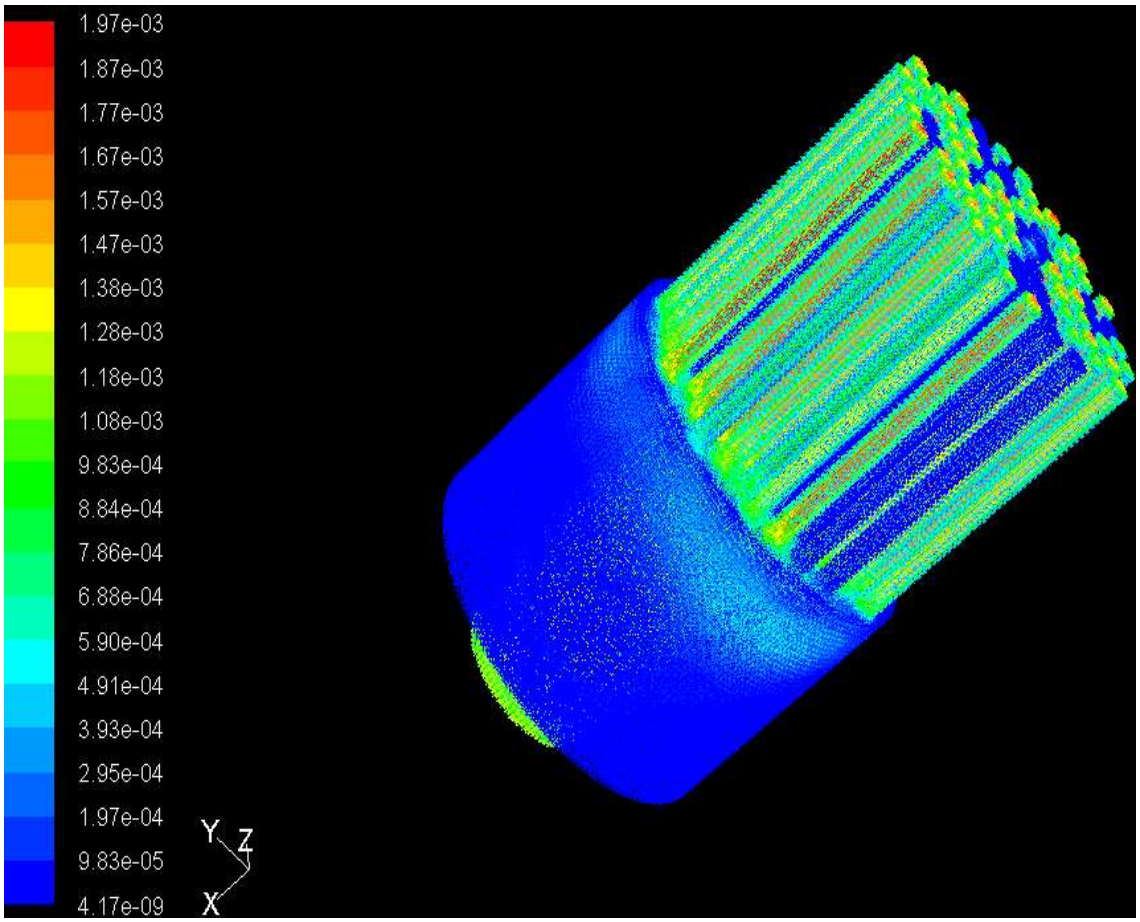

Figure 7 (b). Velocity distribution inside the cylindrical header of L/D = 0.75 with flow rate of Re=1500.

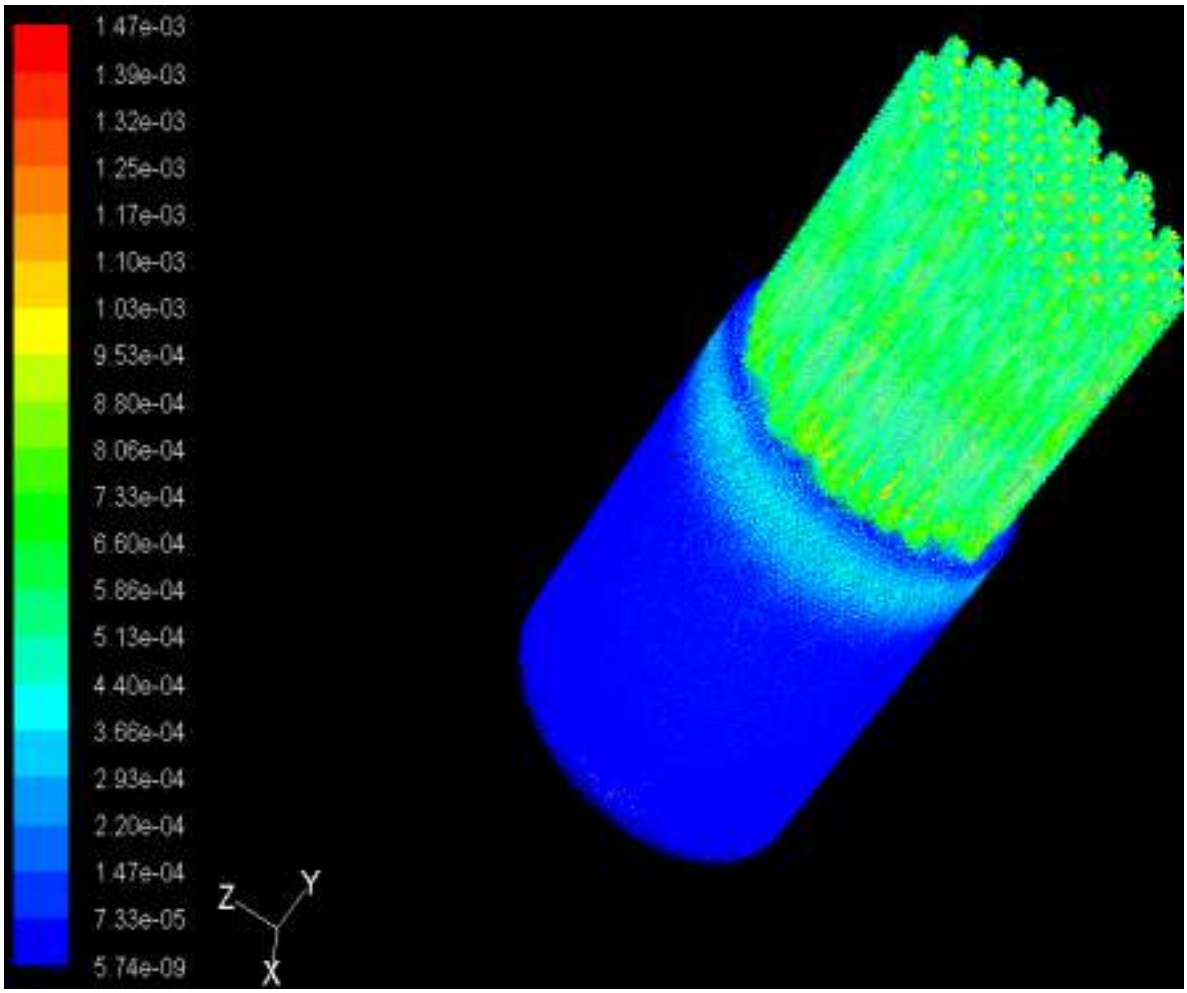

Figure 7 (c). Velocity distribution inside the cylindrical header of L/D = 1.25 with flow rate of Re=1500.

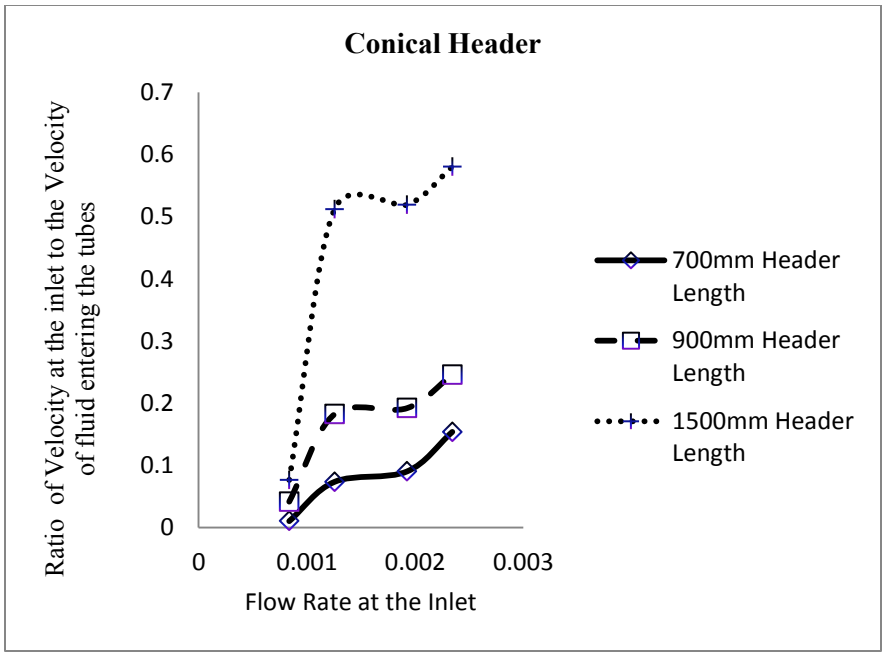

(a)

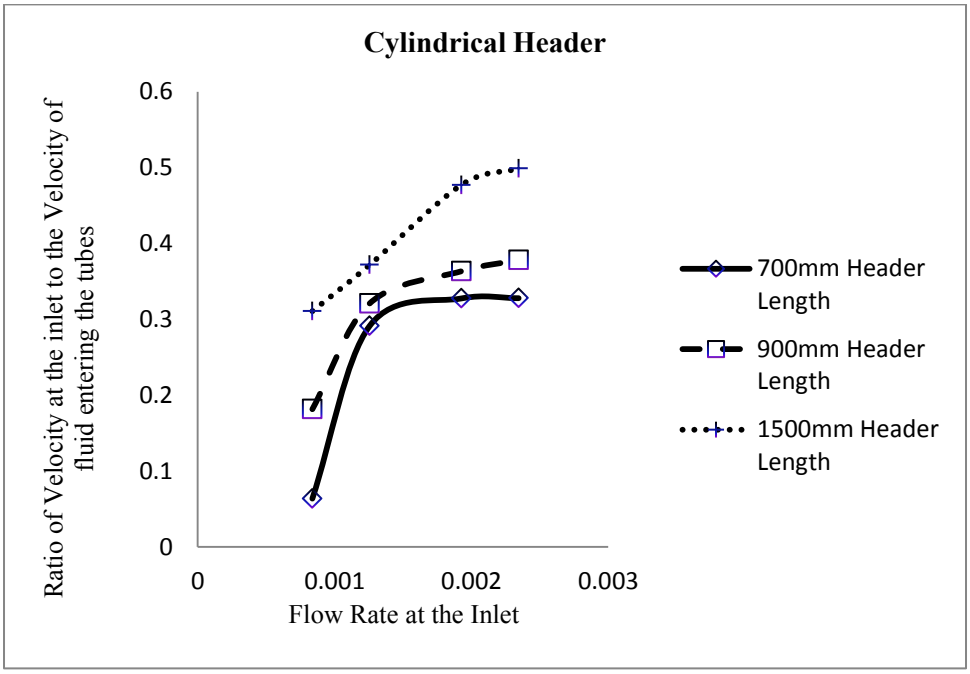

(b)

Figure 8. Flow Rate Vs Velocity: (a) Conical and (b) Circular Header.

5.1.2 Pressure distribution in the header

Figure 9 represents the contours of static pressure inside the conical header part and Figure 10 represents the static pressure distribution inside a circular header part. Figure 9 (a) and (b) represent the pressure distribution inside a conical header with L/D 0.58 and 0.75. It is clear that pressure is not uniformly distributed inside the header and near the entrance to the tubes. It is high near the central zone of the header and gradually decreases towards the corner. Figure 9 (c) shows the pressure distribution in conical header with L/D = 1.25. With increase in L/D of the header maldistribution was minimized, since the pressure distribution was comparatively even for the third case. Figure 10 (a), (b) & (c) shows the pressure distribution in a circular header. The pressure distribution is bad and severe maldistribution takes place. Once more issue that needs to be addressed is the pressure drop along the header length. Though, maldistribution was reduced with increase in length of the header, pressure drop increased rapidly. Figure 11 (a) & (b) represents the graph of ratio of pressure drop to the pressure at the entrance of the tubes to the flow rate. It was identified that the pressure ratio was in the range of 0.1 to 1 for conical headers in comparison to 2 to 20 for circular headers. Though pressure drop increased with length, Figure 11 (a) suggests that the pressure ratio is not very high at higher L/D ratios. More over pressure distribution was much better at higher L/D ratios and this was evident for conical headers. It was deduced that pressure ratio increased by approximately 71 % between L/D 0.58 and 1.25. Since the pressure ratio was high with maldistribution for circular headers, conical headers were preferred over circular ones. Figure 11 illustrates that effect of Reynolds number or flow rate on flow maldistribution. Maldistribution is more severe with increase in Reynolds number. By comparing both the

cases it is clear that conical header with L/D = 1.25 had a minimal flow maldistribution and it is the most effective header type. CFD results are in good agreement with experimental data. Hence CFD technology is capable to closely predict the flow distribution in a shell and tube heat exchanger [40, 41].

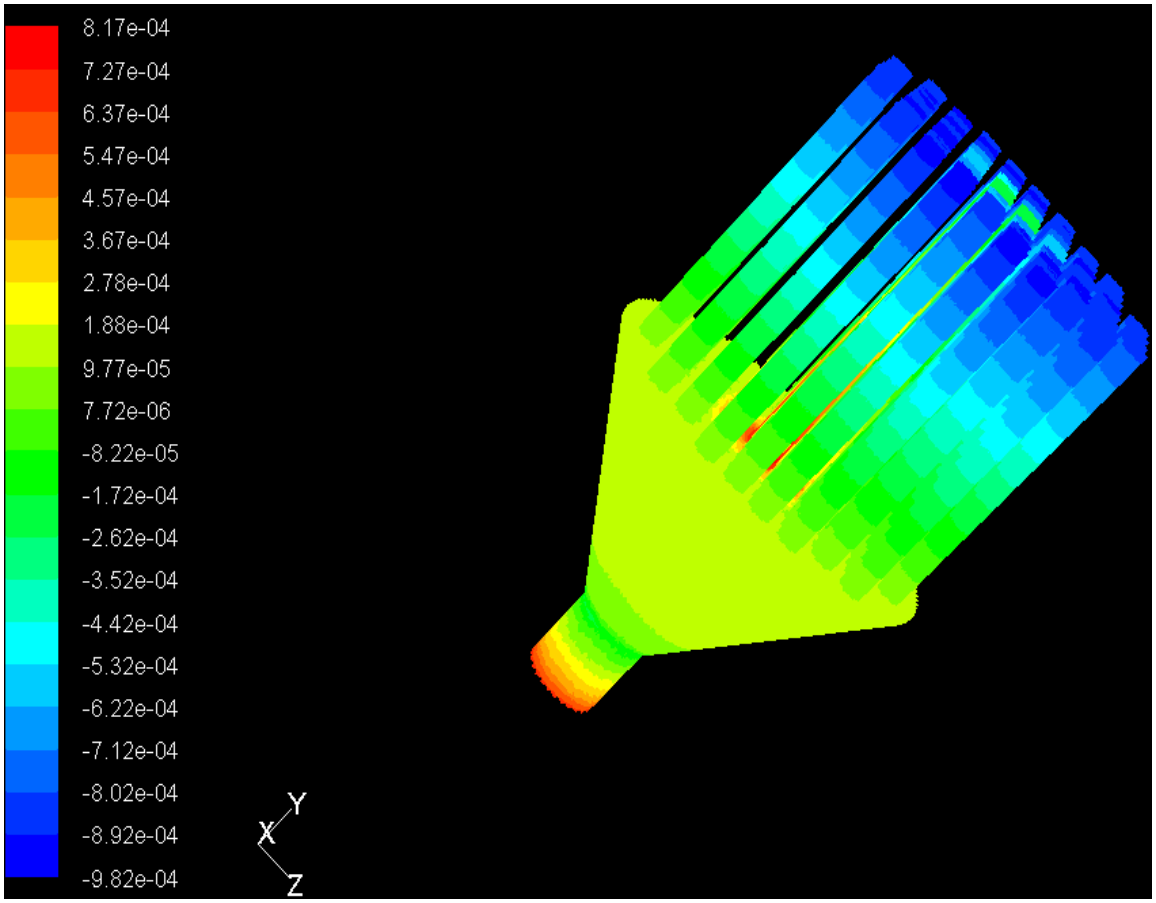

Figure 9 (a). Contours of Pressure distribution inside the conical header of L/D = 0.58 with flow rate of Re=1500.

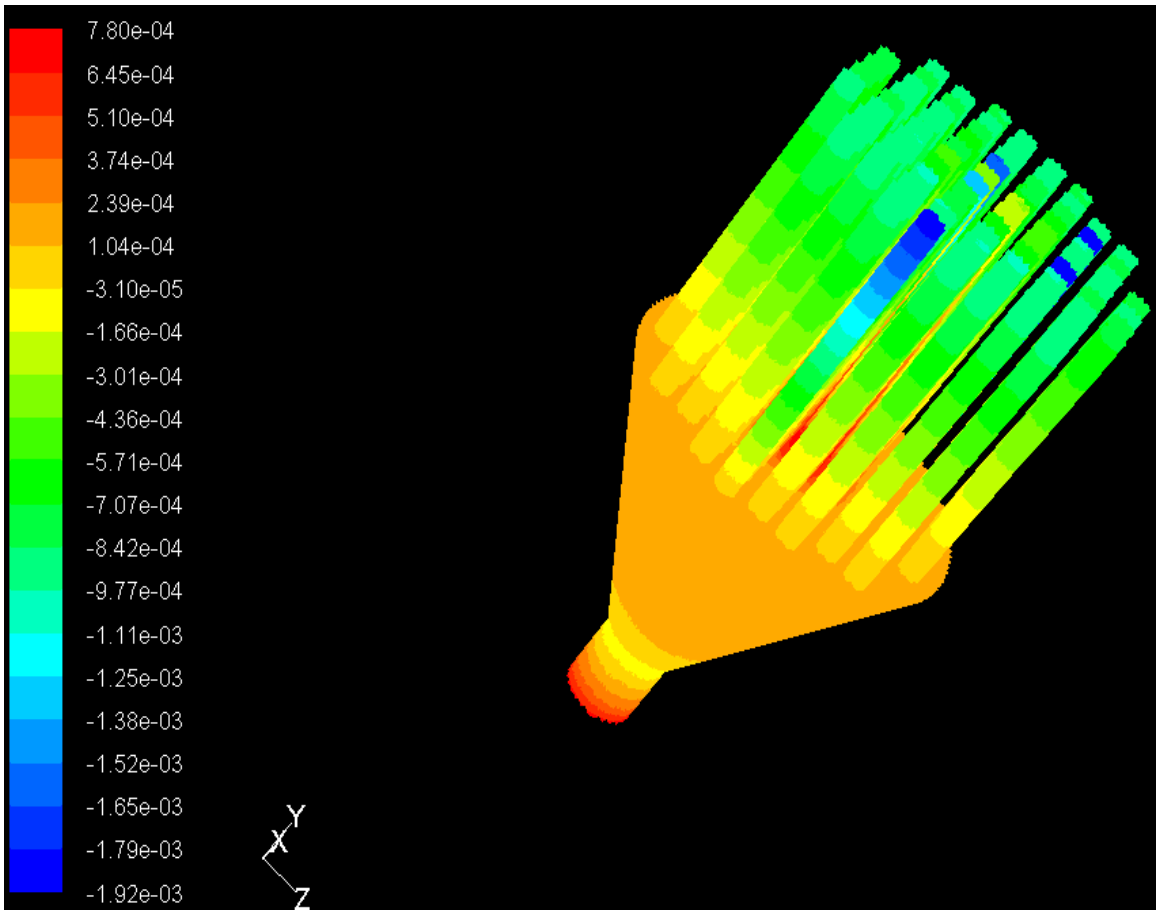

Figure 9 (b). Contours of Pressure distribution inside the conical header of L/D = 0.75 with flow rate of Re=1500.

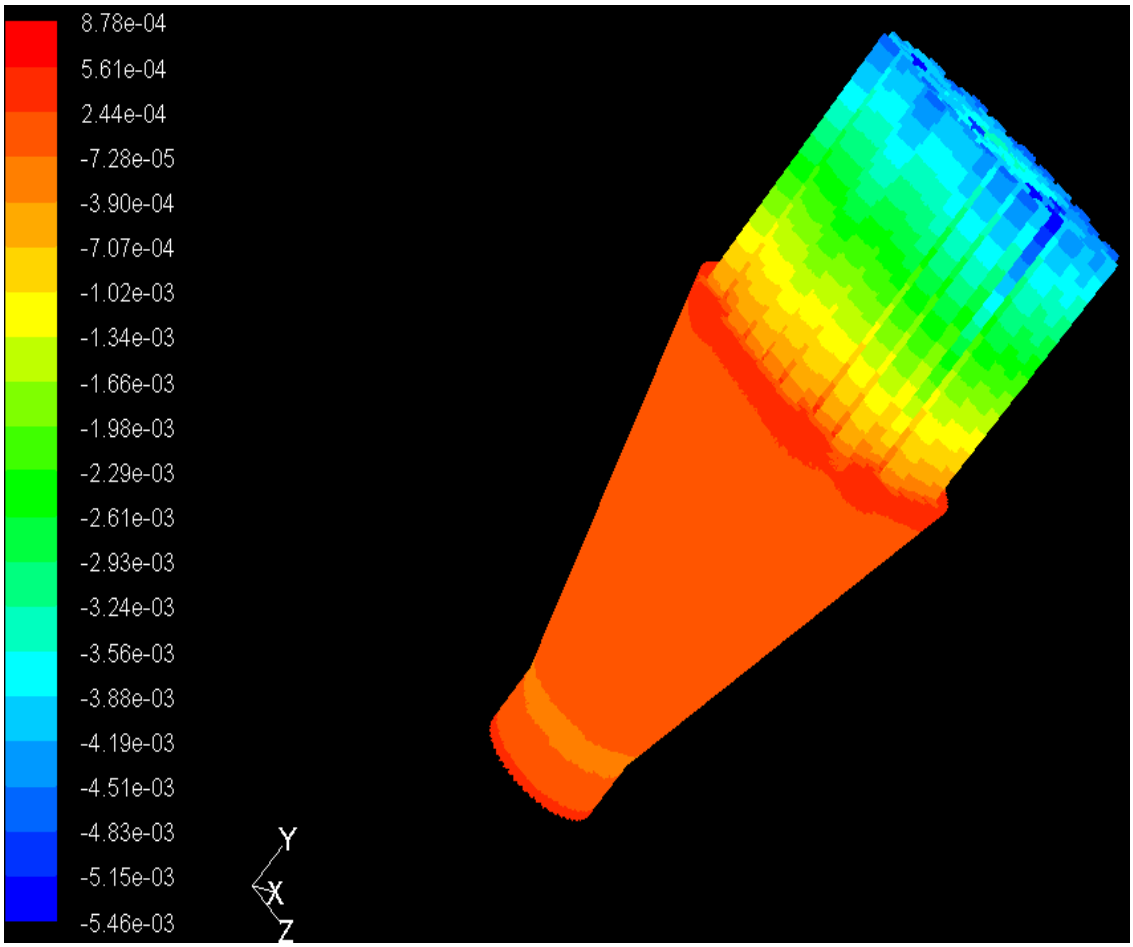

Figure 9 (c). Contours of Pressure distribution inside the conical header of L/D = 1.25 with flow rate of Re=1500.

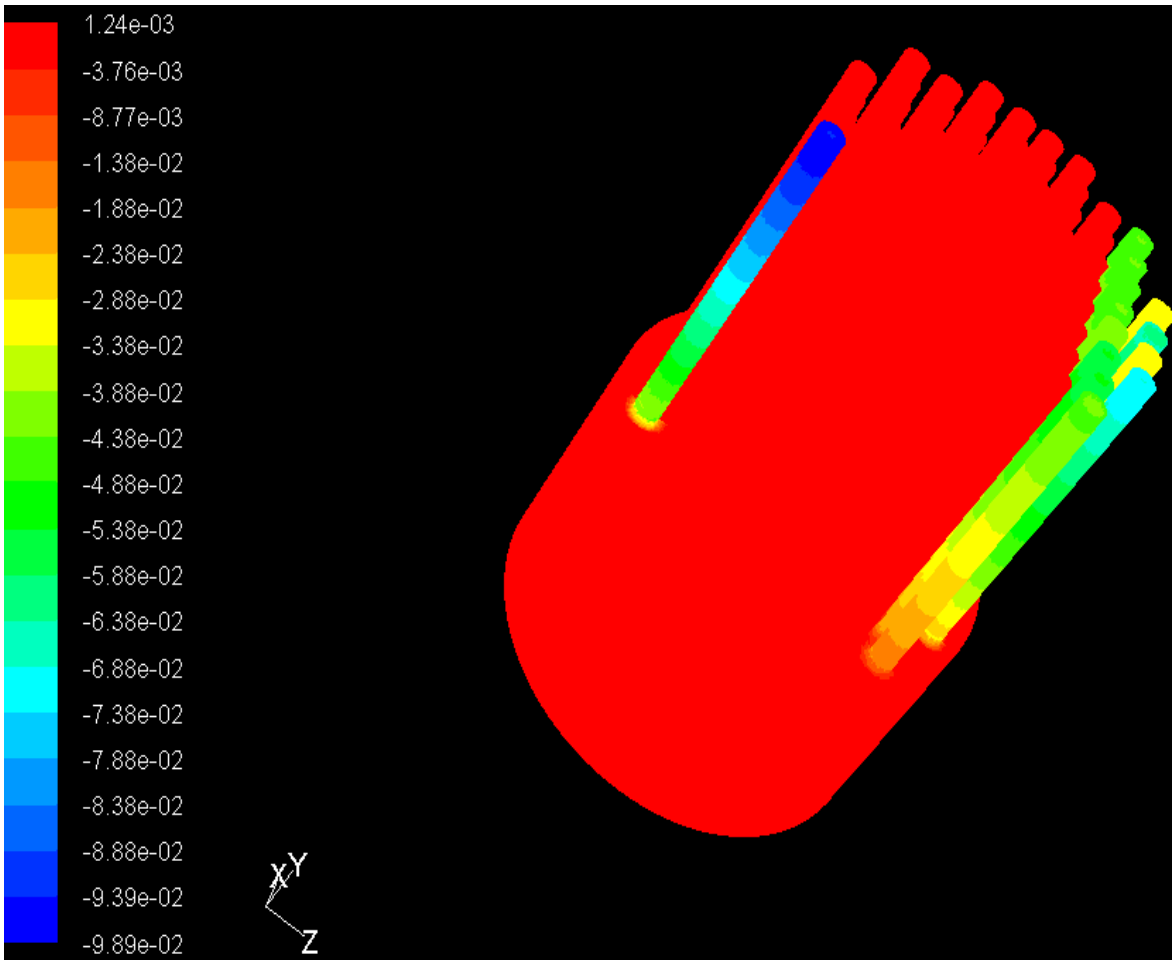

Figure 10 (a). Contours of Pressure distribution inside the circular header of L/D = 0.58 with flow rate of Re=1500

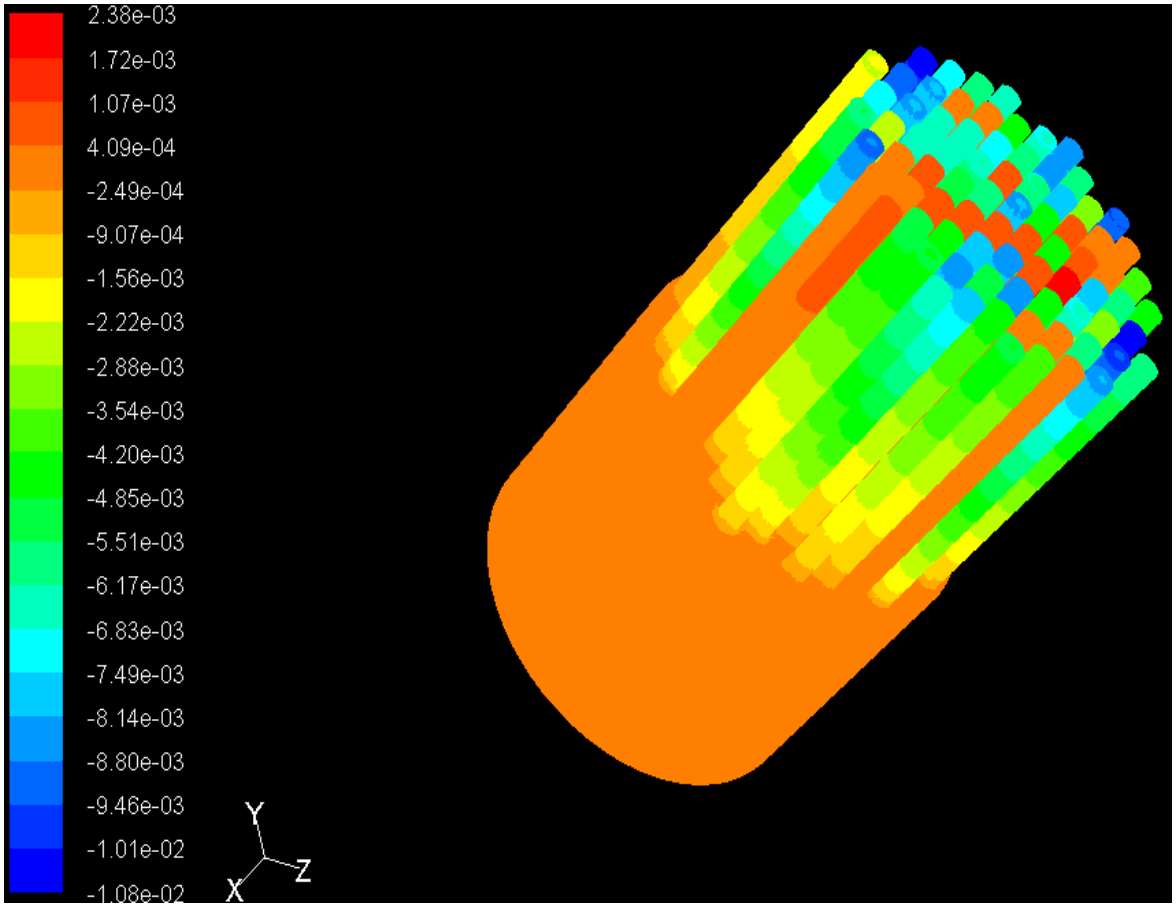

Figure 10 (b). Contours of Pressure distribution inside the circular header of L/D = 0.75 with flow rate of Re=1500

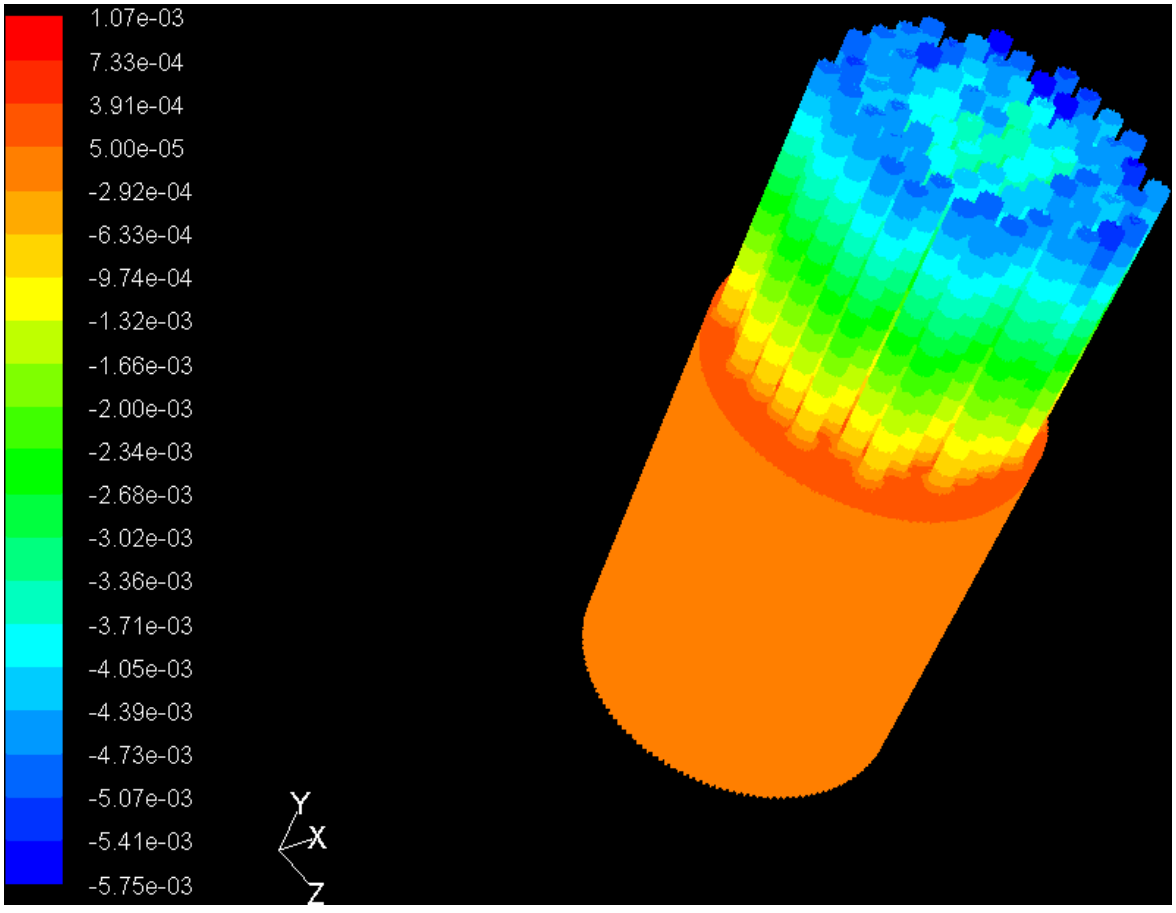

Figure 10 (c). Contours of Pressure distribution inside the circular header of L/D = 1.25 with flow rate of Re=1500

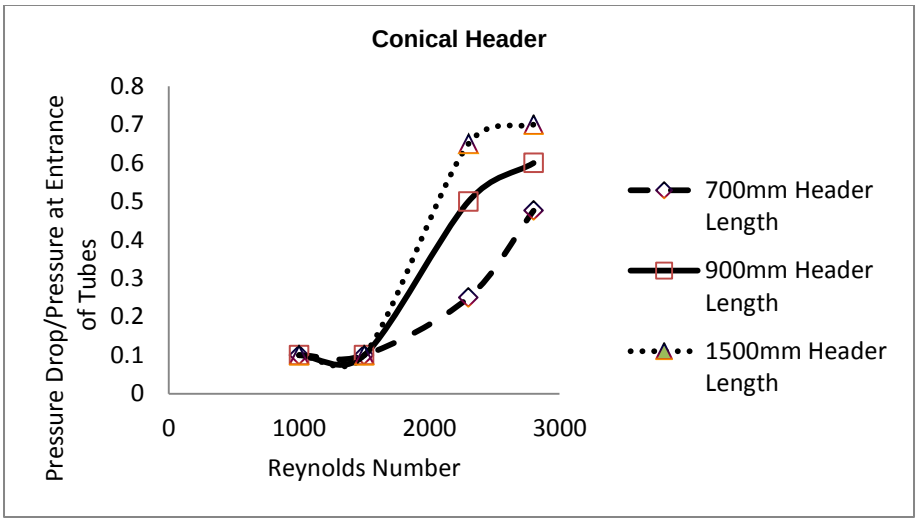

(a)

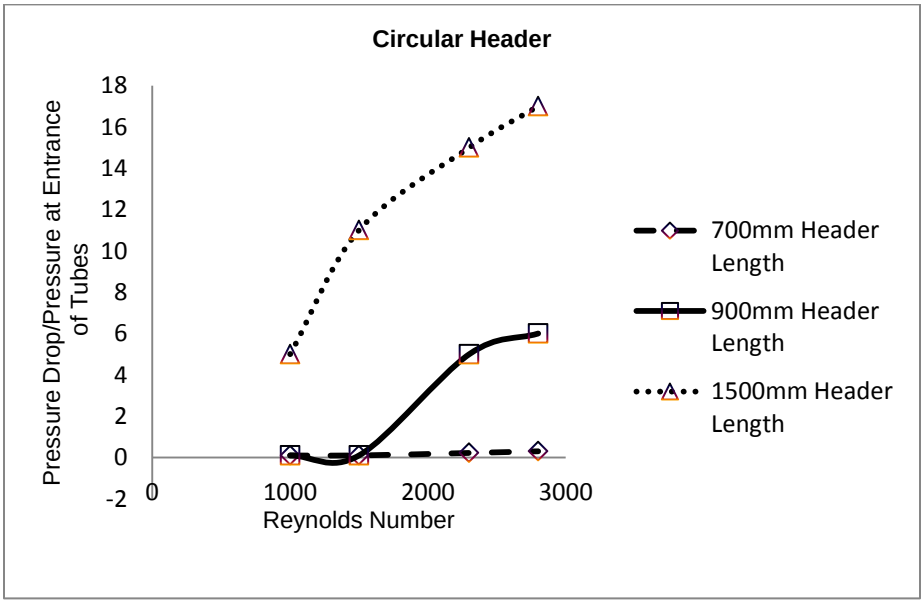

(b)

Figure 11 Reynolds Number Vs Pressure Drop/Pressure at the Entrance of Tubes (a) Conical and (b) Circular Header

5.2 Twisted Tube – Shell Side

Simulations were run for all the four pitch values with three cases of hot fluid. The analysis took a long time to converge due to the complexity in the geometry. In general, pressure drop occurs when there is flow through pipes and this case is no different. It was analyzed that there was a steady drop in pressure inside the twisted tube in call cases. The increase in tube side temperature did not have much of an effect on the shell side pressure although there was a minimal variation in the pressure drop. Also, Figure 12 insisted that the outlet pressure kept decreasing with increase in the fluid velocity (Reynolds number) for the twisted tube model with 5.5D pitch. It was also clear that there was a negligible difference in the outlet pressure for the various tube side temperatures. Interestingly similar results were obtained for other twisted tube models as well. As discussed earlier the outlet pressure decreased with increase in the fluid velocity. When the analysis was run for all cases it was found that for a particular case of the hot fluid, the outlet presure was decreased with decrease in the pitch or helix angle of the twisted tube. Similar results were obtained for other cases of the hot fluid. The reason behind this pressure drop could be the complexity in the geometry. Since the number of twsits increases with decrease in the pitch value, the path of flow may have resulted in high pressure drops. Figure 13 shows the variation of outlet pressure for a hot fluid temperature of 383 K. Similar results were obtained for other hot fluid cases as well.

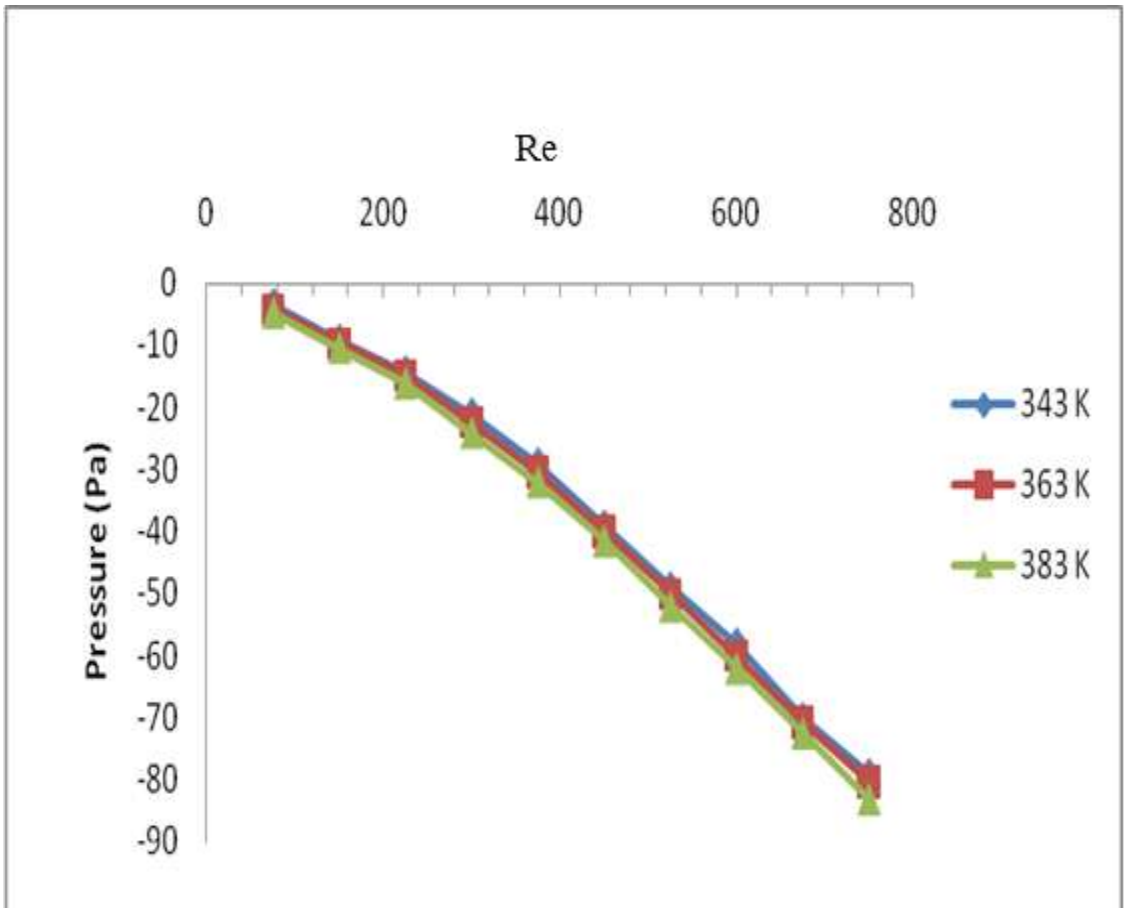

Figure 12. Variation in the outlet pressure at different Re for 5.5D pitch model at various conditions of the hot fluid.

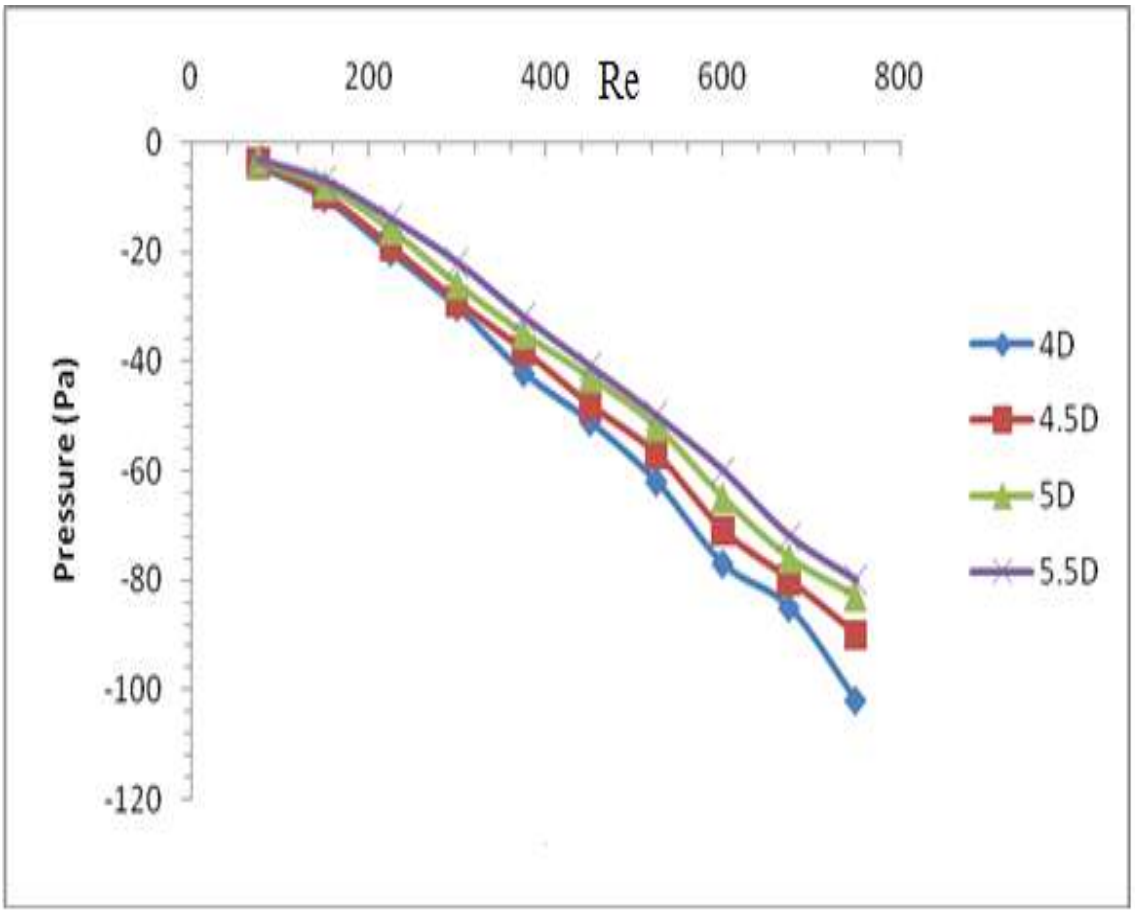

Figure 13. Outlet Pressure at different Re for hot fluid for 383 K.

During the analysis it was observed that the temperature of the cold fluid was high near the walls and gradually decreased towards the center of the channel. It was also seen that with an increase in the Reynolds number the time taken for the fluid to reach its maximum temperature increases. It was analyzed that the average outlet temperature of the fluid decreases with an increase in Reynolds number. At low Reynolds number the fluid reaches the maximum temperature rapidly at a very early stage and maintains the temperature throughout the channel, but with an increase in the Reynolds number the fluid steadily increases to the maximum temperature. It can be clearly seen that the outlet temperature of the fluid decreases with an increase in the Reynolds number. Figure 14 shows the variation of outlet temperature for a twisted tube model with 4D pitch. Similar results were obtained for different pitches. Though the profile of graphs were similar in all cases, the outlet temperature increased with decrease in the pitch, leading to a conclusion that effective heat transfer is achieved with increase in twists. This is well shown in Figure 15.

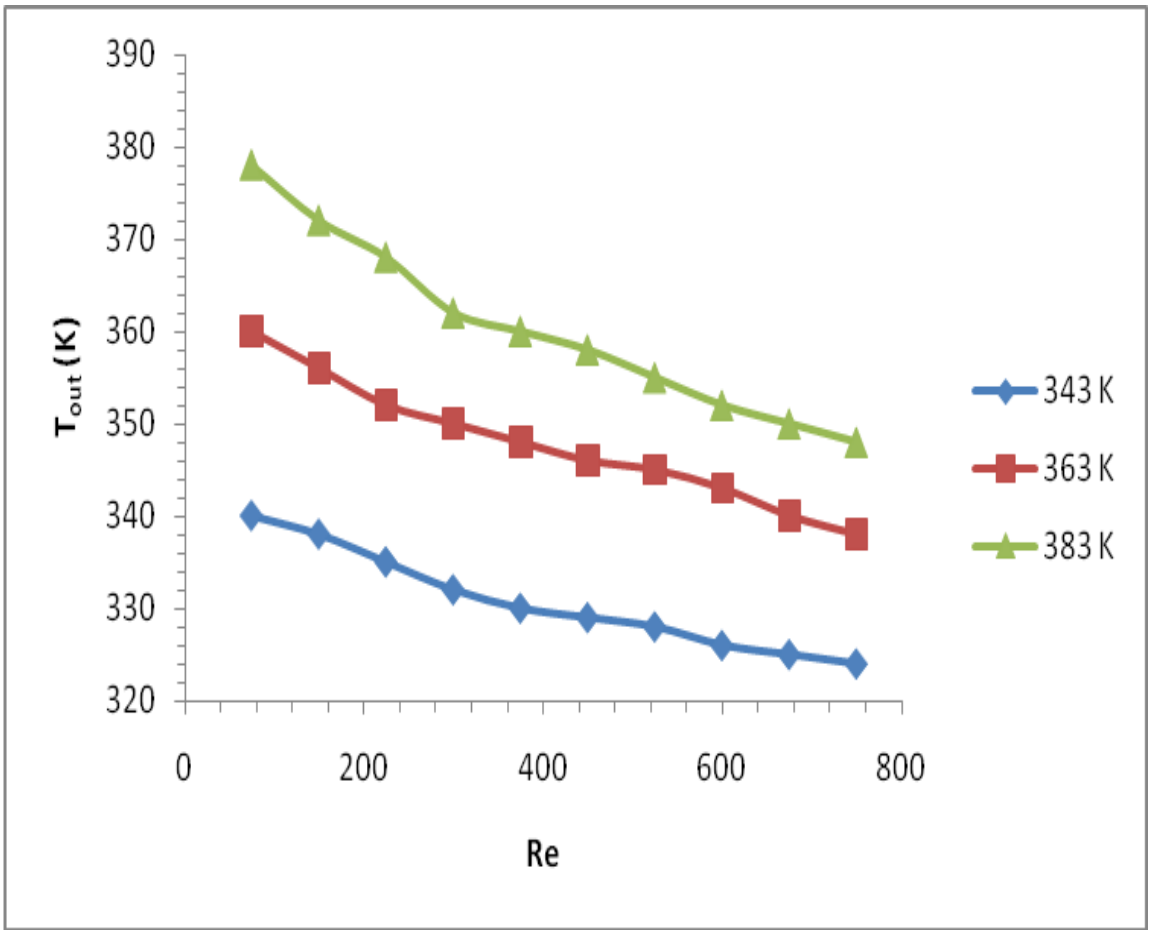

Figure 14. Variation of Outlet Temperature at different Re for a twisted tube with 4D pitch.

Figure 15 shows the variation of the outlet temperature for a hot fluid with CASE 3: 383 K temperatures. It was already discussed that the outlet temperature of the coolant decreases with increase in the Reynolds number. But interestingly, the outlet temperature increases with decrease in the pitch or helix angle of the twisted tube. This figure shows that at all Reynolds number the outlet temperature increases with a decrease in the pitch. This was one of the reasons for which twisted tubes were preferred over conventional cylindrical tubes. It is very evident that with increase in the twist on the tube the outlet temperature of the cold fluid increase and hot fluid decreases.

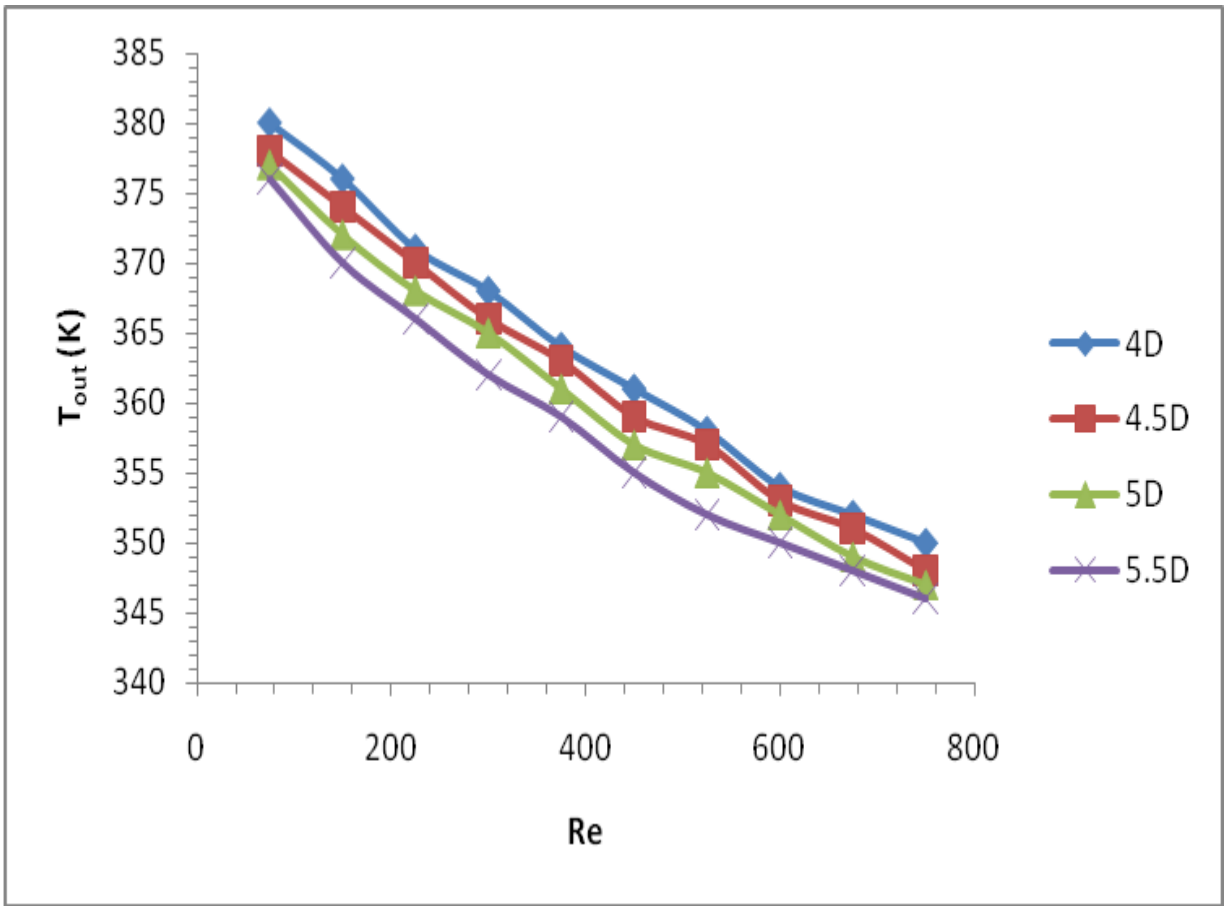

Figure 15. Outlet Temperatures at different Re for 383 K.

The above figures represent the variation of outlet temperatures for different scenarios. But it is always good to calculate the convective heat transfer rate (Q) from the above analysis. Convective heat transfer rate can be determined using the equation (11).

The convective heat transfer was calculated and plotted against Reynolds number. It was quite interesting to find that the convective heat transfer increased with increase in the Reynolds number. The main reason for increase in the heat transfer rate is the decrease in the bulk fluid temperature with increase in the Reynolds number. This was evident in all cases irrespective of the model. Figure 16 shows the variation of convective heat transfer for different Reynolds number for a twisted tube model of 4D pitch. The convective heat transfer rate for different cases of the hot fluid is given in Figure 17. The convective heat transfer rate decreases with decrease in the pitch or helix angle of the tube for all Reynolds number. The main reason for this could be the high temperature of the bulk (cold fluid) at near the outlet. Since the outlet temperature of the cold fluid increases with increase in the twist, the heat transfer rate is forced to decrease due to the fact that the temperature of the bulk cold fluid has a negative sign on the heat transfer formula. This can be clearly seen in Figure 17.

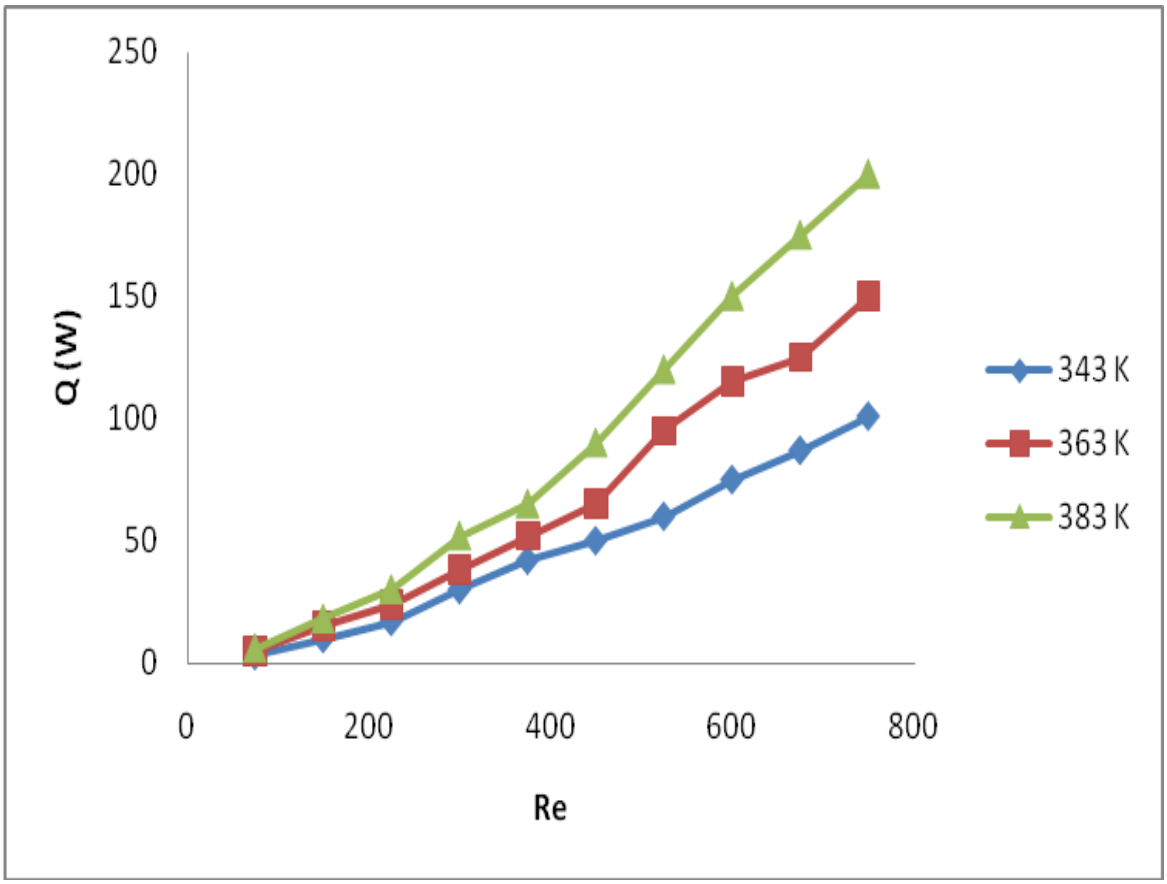

Figure 16. Convective heat transfer rate at different Re for a twisted tube with 4D pitch.

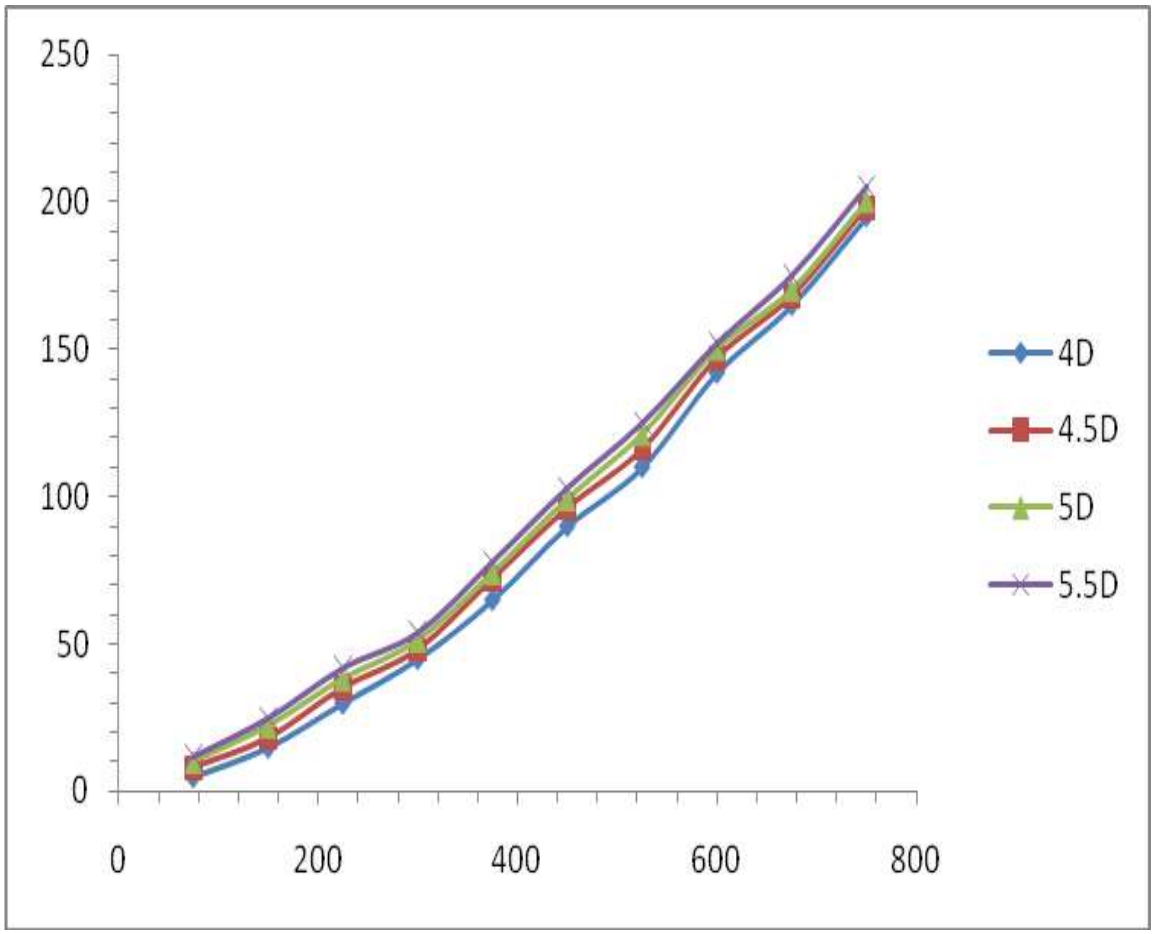

Figure 17. Convective heat transfer rate at different Re for hot fluid of 383 K.

5.3 Discussions

The above results clearly suggest that maldistribution is high at small ratios of L/D. Also, the increase in twist angle of the tubes increases the shell side heat transfer performance. Although, heat transfer performance is given more prominence in this paper other factors like pressure drop should be addressed. One reason for this could be the increase in cost incurred in handling the pressure drop. From figure 8 it was evident that velocity distribution was more uniform for higher Reynolds number at larger L/D ratios of the header. This is very important in terms of the mass flow through each tube as that affects the heat transfer performance of the heat exchanger. Also, figure 11 briefs the effect of length and Reynolds number on pressure drop inside the header. It was obvious that conventional cylindrical headers had a higher pressure drop rate than conical ones for a given condition. Though the pressure is drop is comparatively less in conical headers than in cylindrical ones, the amount of pressure drop is still high which is not advisable. But the system is still considered because emphasis was given on uniform pressure distribution at the inlet of all tubes. In order to overcome this issue, pumps can be used. These pumps can be used to reduce the pressure drop inside the heat exchanger. Installing pumps to control pressure drop would not be as expensive as having an heat exchanger with low heat transfer performance, because the cost incurred on that would be more than the former. Also, the shell side flow is analyzed for its heat transfer performance. In doing that figure 13 clearly shows that high pressure drops prevail in cases with higher twist angles (small pitch). But it was also identified that the heat transfer performance improved with increase in twist angle. Again pressure drop is the only concern and it can be taken care of by use of pumps. One more important factor that can be addressed would

include the effect of maldistribution of flow in the header on the shell side heat transfer. When there is maldistribution in fluid flow in the header, fluid is not evenly distributed among the tubes. This would result in poor heat transfer between the hot and cold fluid. It is well known that equal volume of fluid should flow through all the tubes, such that when the cold fluid passes over the tubes on the shell side, heat transfer takes place. But in most cases maldistribution takes place and results in unequal distribution of fluid in the tubes. If this can be analyzed, then the percentage of improvement in heat transfer can also be identified based the difference in heat transfer between fluid flow during maldistribution and uniform distribution.

CHAPTER 6

CONCLUSIONS AND FUTURE WORK

6.1 Conclusions

The analysis of flow maldistribution and heat transfer characteristics in a shell and tube heat exchanger is presented. The uniformity of flow distribution was increased with increase in header length, where as it decreased with increase in flow rate. Maldistribution of flow in the header affects the heat transfer performance. So, the effects of the pressure drop, velocity distribution in the header part were analyzed. In some of tubes as there is non - uniformity in the distribution of flow the pressure drop is less. It is also evident that with the increase in the flow rate the pressure drop is increasing. With the increase in the header length the pressure drop increased and the pressure is high at higher Reynolds numbers. It is found that the pressure drop in the high flow rate passages would be higher than those in the low flow rate passages due to the flow maldistribution in the header part of shell and tube heat exchanger. With the increase in the flow rate the velocity is increasing. With the increase in the header length flow maldistribution which is obvious and the velocity is high at higher Reynolds numbers. To increase the performance of the heat exchanger maldistribution of flow among the tubes should not be present. So by changing the geometry of the header part according to that will lead to better results. As the header length is increased to 1500mm the flow maldistribution was reduced and the static pressure was almost equal for all the tubes. So from this we can conclude that conical header with 1500mm header length has less flow maldistribution when compared to other models. CFD analysis of a twisted tube for a STHE was carried out in order to model the shell side of a shell and tube heat exchangers. The simulations

were run for four models of the twisted tube with pitch varying from 4D to 5.5D. The analysis was also run at three different hot fluid temperatures as in 343K, 363K and 383K. The following results were drawn from the simulation.

- In all cases there was a steady drop of pressure with increase in the Reynolds number.
- Pressure drop across the twisted tube increased with the increase decrease in pitch. The reason for this could be the increasing number of twists on the tube with decreasing pitch.
- As expected outlet temperature of the bulk cold fluid decreased with increase in Reynolds number in all cases. It was evident that the outlet temperature increased with decrease in the pitch of the twisted tube. This showed that twisted tube have higher heat transfer coefficient.

As per theory convective heat transfer rate increases with increase in fluid motion and all cases followed the same pattern. It was also found that convective heat transfer rate increases with increase in the pitch owing to the decrease in outlet temperature.

6.2 Future Work

Based on the results obtained in this paper, the following works can be considered to extend the knowledge on shell and tube heat exchangers.

- The working fluids can be changed in both the tube side and shell side of the STHE.
- The inlet to the header can be optimized by changing its position.

- The shell side flow is considered as flow through a twisted in this paper, as it is an attempt to analyze shell side flow with twisted tubes. In the future shell side flow can be modeled with tubes and flow can be analyzed as flow over the tubes itself.

REFERENCES

REFERENCES

1. Retrived on 02/03.2011 at: http://www.softpedia.com/progScreenshots/Shell-and-Tube-Heat-Exchanger-Screenshot-71424.html

2. Sadik K, Hongtan L, 2002, "Heat Exchangers Selection, Rating and Thermal Design," Book, Second Edition.

3. Myoung, k., young, L., Byung, K., Dong, L., and Won, S., 2009, "CFD modeling of shell and tube heat exchanger header for uniform distribution among the tubes," Korean J.Chem.Eng., **26**(2), pp. 359-363.

4. J.W.palen.,1986, Heat transfer source book

5. Wolverine tube Inc. Engineering Data book 3.

6. Wang, Q., Chen, Q., Chen, G., and Zeng, M., 2009, "Numerical investigation on combined multiple shell-pass shell-and-tube heat exchanger with continuous helical baffles," International Journal of Heat and Mass Transfer **52**, pp. 1214-22.

7. Mueller A.C..,1987,"Effects of some types of maldistribution on the performance of heat exchangers", Heat Transfer Engineering, **8(**2), pp.75-86.

8. Patankar S.V., Spalding D.B.., 1974, "A calculation procedure for the transient and steady state behavior of shell-and- tube heat exchanger", in N.F. Afgan, E.U. Schlunder(Eds.),Heat Exchanger Design and Theory Source Book,. McGraw-Hill, New York, pp.44-60.

9. Butterworth. D., 1978, "A model for heat transfer during three-dimensional flow in tube bundles", 6th International Heat Transfer Conference, Toronto, August.

10. Mueller AC, Chiou JP., 1988,"Review of various types of flow maldistribution in heat Exchangers", J Heat Transfer Eng, **9**(2),36–50.

11. Fraas A.P., 1989, "Thermodynamic design optimization of a heat recuperator", Heat exchanger design, 2nd Ed., Wiley, New York.

12. Ranganayakulu C, Seetharamu KN, Sreevatsan KV.,1997, "The effects of inlet fluid flow nonuniformity on thermal performance and pressure drops in crossflow plate-fin compact heat exchangers", Int J Heat Mass Transfer, **40**(1), pp.27–38.

13. Zhang Z.G., Xu T., Fang X.M..,2004," Experimental study on heat transfer enhancement of a helically baffled heat exchanger combined with three-dimensional finned tubes, Appl. Thermal Eng. 24, pp. 2293–2300.

14. Jian-Fei Z, Ya-Ling He, Wen- Quan T.,2009,“ 3D numerical simulation on shell-and-tube heat exchangers with, middle-overlapped Numerical model and results of whole heat exchanger with middle-overlapped helical baffles, “International Journal of Heat and Mass Transfer **52**, pp.5371–5380.

15. Zhang Z, Zhong L., 2003,“ CFD simulation on inlet configuration of plate-fin heat exchangers,” Cryogenics., **43,** pp. 673–78.

16. Peng B., Wang Q.W., Zhang C., Xie G.N., Luo L.Q., Chen Q.Y., Zeng M..,2007, “An experimental study of shell-and-tube heat exchangers with continuous helical baffles,” ASME J. Heat Transfer **129** , pp.1425–1431.

17. Yong G. L, Ya-Ling H, Pan C., 2008 exchangers with helical baffles”, Chem. Eng. Sci. **63**, pp. 4386–4395.

18. Prithiviraj M., Andrews M.J.., 1998, “Three-dimensional numerical simulation of shell and-tube heat exchanger, Part I: foundation and fluid mechanics, Numer. Heat Transfer A Appl”, **33**, pp. 799–816.

19. Prithiviraj M., Andrews M.J..,1998, “Three-dimensional numerical simulation of shell and- tube heat exchanger, Part II: heat transfer, Numer. Heat Transfer A Appl”, pp. 817–828.

20. Prithiviraj M., Andrews M.J..,1999, “Comparison of a three-dimensional numerical model with existing methods for prediction of flow in shell-and-tube heat exchangers”, Heat Transfer Eng. **20** (2), pp.15–19.

21. Bin D., 2003, “Experimental and numerical study of flow and heat transfer in the shell side of heat exchangers, Ph.D. dissertation, Xi’an Jiaotong University, Xi’an, China.

22. Andrews M.J., Master B.I..,1999, “3-D modeling of the ABB Lummus Heat Transfer Helix changer using CFD”, International Conference Compact Heat Exchangers, Banff, Canada, July pp.19–23,

23. Andrews M.J., Master B.I.., 2005, “Three-dimensional modeling of a Helix changer heat exchanger using CFD”, Heat Transfer Eng. **26**, pp. 22–31.

24. Schröder K., Gelbe H..,1999, “Two- and three-dimensional CFD-simulation of flow induced vibration excitation in tube bundles”, Chem. Eng. Process. **38**, pp. 621–629.

25. Karlsson T., Vamling L.., 2005, “Flow fields in shell-and-tube condensers: comparison of a pure refrigerant and a binary mixture”, Int. J. Refrigeration,**28**, pp. 706 – 713.

26. Lee S.H., Hur N..,2007, “Numerical analysis of the fluid flow and heat transfer in a shell and tube heat exchanger”, Proceedings of 1st Asian Symposium on Computational Heat Transfer and Fluid Flow, Xi’an, China, October, pp.18–21.

27. Shen R.J., Feng X., Gao X.D.., 2004, “Mathematical model and numerical simulation of helical baffles heat exchanger”, J. Enhanced Heat Transfer **11**, pp.461–466.

28. Yong-Gang L, Ya-Ling H, Rui L, Ya-Fu Gao.,2008,“Effects of baffle inclination angle on flow and heat transfer of a heat exchanger with helical baffles”, Chem. Eng. Process. Process Intensification **47** (12), pp.2336–2345.

29. Jafari Nasr M.R., Shafeghat A..,2008, “Fluid flow analysis and extension of rapid design algorithm for helical baffle heat exchangers”, Appl. Thermal Eng. **28**, pp.1324–1332.

30. Uo X, Roetzel W., 1998, “Theoretical investigation on cross-flow heat exchangers with axial dispersion in one fluid”, 37(3), pp. 223–33.

31. Chen H, Cao C, Xu LL, Xiao TH, Jiang GL.,1998, Experimental velocity measurements and effect of flow maldistribution on predicted permeator performances. J Membr Sci; **139**(2).,pp. 259–68.

32. Thonon B, Mercier P., 1996, Plate heat exchangers: ten years of research at GREThe. 2.Sizing and flow maldistribution.Revue Generale de Thermique;**35**(416), pp.561–8.

33. Ratts EB.,1998, “Investigation of flow maldistribution in a concentric-tube,Counterflow, laminar heat exchanger”, Heat Transfer Eng, **19**(3), pp.65–75.

34. Vist S. and.Pettersen J.,2004, “Experiments on two-phase flow distribution inside parallel channels of compact heat exchangers”, Exp.Therm. and Fluid Sci., **28**, pp. 209.

35. Lalot S.,.Florent P, S.K.Lang and A.E.Bergles.,1999,“Determination of apparent heat transfer coefficient by condensation in an industrial finned-tube heat exchanger prediction” ,Appl. Therm.Eng**.,19**,pp.847.

36. Jiang-Tao L, Xiao-Feng P, Wei-Mon Y, 2007 Numerical study of fluid flow and heat transfer in microchannel cooling passages. International Journal of Heat and Mass Transfer 50 , pp.1855–1864.

37. Jung-Yeul J., Ho-Young K, 2008. Fluid flow and heat transfer in microchannels with rectangular cross section. Heat Mass Transfer, 44, pp.1041–1049

38. Poh-Seng L, Garimella S.V, Dong L. 2005, Investigation of heat transfer in rectangular microchannels. International Journal of Heat and Mass Transfer 48, pp. 1688–1704.

39. Gian L, Morini Gian L, 2004. Single-phase convective heat transfer in microchannels: a review of experimental results. International Journal of Thermal Sciences 43, pp. 631–651.

40. Gopinath R. W, Vijay K. D, Leslie A. M, 2002. Heat transfer and pressure drop in narrow rectangular channels. Experimental Thermal and Fluid Science 26, pp. 53–64.

41. Stephen A. S, Ljubisa D S, Richard A, 2006. Beaupre Microchannel takes heat sink to next level. Power Electronics November.

42. Celata G.P., Cumo M, Marconi V., McPhail S.J., Zummo G, 2006. Microtube liquid single-phase heat transfer in laminar flow. International Journal of Heat and Mass Transfer 49, pp.3538–3546

43. Zeng-Yuan G, Zhi-Xin L, Size effect on single phase channel flow and heat transfer at micro scale. 2003. International Conference of heat an fluid flow. 24, pp.284-298.

44. Tiselj, Hetsroni G, Mavko B, Mosyak A, Pogrebnyak E, Segal Z, 2004. Effect of axial conduction on the heat transfer in micro-channels., International Journal of Heat and Mass Transfer 47, pp. 2551–2565.

45. Qu W, Mudawar I, 2002. Analysis of three-dimensional heat transfer in micro-channel heat sinks, Int. J. Heat Mass Transfer 45, pp. 3973–3985.

46. Garimella S, 2003. Condensation flow mechanisms in microchannels: basis for pressure drop and heat transfer models Proc. 1st Int. Conf. Microchannels and Minichannels (ASME, Rochester, NY) pp 181–92.

47. Coleman, J. W., and Garimella, S., Characterization of Two- Phase FlowPatterns in Small Diameter Round and Rectangular Tubes, Int. J. Heat and Mass Transfer, vol. 42, no. 15, pp. 2869–2881, 1999.

48. Zhao T S and Liao Q 2002 Theoretical analysis of film condensation heat transfer inside vertical mini triangular channels Int. J. Heat Mass Transfer 45, pp. 2829–42.

49. Wang W, Radcliff T D and Christensen R N, 2002. A condensation heat transfer correlation for millimeter-scale tubing with flow regime transition Exp. Therm. Fluid Sci. 26, pp. 473–485.

50. Kim M H, Shin J S, Huh C, Kim T J and Seo K W 2003 A study of condensation heat transfer in a single mini-tube and a review of Korean micro- and mini-channel

studies Proc. 1st Int. Conf. Microchannels and Minichannels (ASME, Rochester, NY) pp 47–58.

51. Yang C.Y, Webb R.L, 1996. Condensation of R-12 in small hydraulic diameter extruded aluminum tubes with and without micro-fins, Int. J. Heat Mass Transfer 39, pp. 791-800.

52. Garimella, T. Bandhauer, *Measurement of Condensation Heat Transfer Coefficients* in Microchannel Tubes, Proc. of the 2001 International Mechanical Engineering Congress and Exposition, ASME Heat Transfer Division HTD-24221, 2001, p. 1.

53. Fiedler S., Auracher H., 2001 Proc. of 3rd Int. Conf. on Compact Heat Exchangers and Enhancement Technology for the Process Industries, pp. 369-375

54. Shin, J.S., Kim, M.H., 2004. An experimental study of condensation heat transfer inside mini-channels with a new measurement technique. Int. J. Multiphase Flow 30, pp. 311–325.

55. Wang, H.S., Rose, J.W., Honda, H., 2004. A theoretical model of film condensation in square section horizontal microchannels. Chem. Eng. Res. Des. 82, pp. 430–434.

56. Me´de´ric, B., Lavieille, P., Miscevic, M., 2005. Void fraction invariance properties of condensation flow inside a capillary glass tube. Int. J. Multiphase Flow 31, pp. 1049–1058.

57. Baird, J.R., Fletcher, D.F., Haynes, B.S., 2003. Local condensation heat transfer rates in fine passages. Int. J. Heat Mass Transf. 46, pp. 4453–4466.

58. Garimella, S., Agarwal, A., Killion, J.D., 2005. Condensation pressure drop in circular microchannels. Heat Transf. Eng. 26, pp. 28–35.

59. Louahlia-Gualous, H., Mecheri, B., 2007. Unsteady steam condensation flow pattern inside a miniature tube. Appl. Therm. Eng. 27, pp. 1225–1235.

60. Wei Z, Jinliang X, Guohua L., 2008. Multi-channel effect of condensation flow in a micro triple-channel condenser. Int. J. Multiphase flow, 34, pp. 1175-1184

61. Huiying W, Xinyu W, Jian Q and Mengmeng Y., 2008. Condensation heat transfer and flow friction in silicon microchannels. J. Micromech. Microeng. 18, 115024 (10pp)

62. Simin W, Jian W, and Yanzhong L, 2009**.** An experimental investigation of heat transfer enhancement for a shell-and-tube heat exchanger. Applied Thermal Engineering, 49, pp. 2433-2438

63. Chen, G. D, Chen, Q. Y, Min W, Qiu-W, 2009. Numerical studies on combined multiple shell-pass shell- and-tube heat exchanger with helical baffles. Journal of Engineering Thermophysics, 30, pp. 1357-1359.

64. Keene, L.W., Davies, T.W. and Gibbons, D.B., 1993. Flow distribution on the shellside of a shell and tube heat exchanger. Chemical Engineering Research and Design, 71, pp 310-311.

65. Ozden, Ender and Tan, Ilker, 2008. CFD modeling and analysis of a shell-and-tube heat exchanger Proceedings of the ASME Summer Heat Transfer Conference, HT 2008, pp 75-76, 2009, 2008 Proceedings of the ASME Summer Heat Transfer Conference, HT 2008.

66. Jiyuan T, Guan H. Y, Chaoqun L, "Compuatational fluid dynamics", A practical approach, Elsevier publications.

67. Patakar S.V., (1980), "Numerical Heat Transfer and Fluid Flow", McGraw-Hill Company, New York.

68. FLUENT version 6.3.26 Manual, 2004.

69. Tao W.Q..,2001, Numerical Heat Transfer, second ed., Xi'an Jiaotong University Press, Xi'an, China.

70. Habib M.A, Ben-Mansour R. , Said S.A.M., Al M.S, Qahtani , Al-Bagawi J.J., Al-Mansour K.M.., 2009," Evaluation of flow maldistribution in air-cooled heat exchangers," Computers & Fluids.,**38,pp**.677–690.